HIGH-DENSITY PLASMA ETCHING OF MAGNETIC DEVICES

By

KEE BUM JUNG

A DISSERTATION PRESENTED TO THE GRADUATE SCHOOL
OF THE UNIVERSITY OF FLORIDA IN PARTIAL FULFILLMENT
OF THE REQUIREMENTS FOR THE DEGREE OF
DOCTOR OF PHILOSOPHY

UNIVERSITY OF FLORIDA

1999

Trust in the Lord with all your heart
and lean not on your own understanding;
in all your ways acknowledge him
and he will make your paths straight.

Proverbs 3:5-6

ACKNOWLEDGMENTS

First and foremost, I would like to express great appreciation with all my heart to Professor Pearton for his expert advice, guidance, and instruction throughout the research. I also give special thanks to members of my committee–Professor Abernathy, Professor Sharifi in Department of Physics, Professor Singh, Professor Ren, and Dr. Childress at IBM Almaden Research Center in San Jose, CA–for their professional input and support. Additional special thanks are reserved for the people of our research group–Dr. Hahn, Dr. Cho, X. Cao, D. C. Hays, P. Leerungnawarat, K. P. Lee, and J. Marburger in the Department of Physics–for their assistance, care, and friendship. I am very grateful to past group members–Dr. C. B. Vartuli, Dr. J. W. Lee, Dr. J. Hong, and J. J. Wang. I also give my thanks to P. Mathis for her endless help and kindness.

I am always thankful for God's help and blessing for me to be where I am today. In addition, I give my sincere gratitude to my parents and parents-in-law for their unlimited love and encouragement, and especially to my lovely wife, Heesun Kim Jung, for her emotional help, inspiration, and continual prayers.

TABLE OF CONTENTS

LIST OF TABLES

LIST OF FIGURES

Abstract of Dissertation Presented to the Graduate School
of the University of Florida in Partial Fulfillment of the
Requirements for the Degree of Doctor of Philosophy

HIGH DENSITY PLASMA ETCHING OF MAGNETIC DEVICES

By

Kee Bum Jung

August 1999

Chairman: Stephen J. Pearton
Major Department: Materials Science and Engineering

Magnetic materials such as NiFe (permalloy) or NiFeCo are widely used in the data storage industry. Techniques for submicron patterning are required to develop next-generation magnetic devices. The relative chemical inertness of most magnetic materials means they are hard to etch using conventional RIE (Reactive Ion Etching). Therefore ion milling has generally been used across the industry, but this has limitations for magnetic structures with submicron dimensions. In this dissertation, we suggest high density plasmas such as ECR (Electron Cyclotron Resonance) and ICP (Inductively Coupled Plasma) for the etching of magnetic materials (NiFe, NiFeCo, CoFeB, CoSm, CoZr) and other related materials (TaN, CrSi, FeMn), which are employed for magnetic devices like magnetoresistive random access memories (MRAM), magnetic read/write heads, magnetic sensors and microactuators. This research examined the fundamental etch

mechanisms occurring in high density plasma processing of magnetic materials by measuring etch rate, surface morphology and surface stoichiometry.

However, one concern with using Cl_2-based plasma chemistry is the effect of residual chlorine or chlorinated etch residues remaining on the sidewalls of etched features, leading to a degradation of the magnetic properties. To avoid this problem, we employed two different processing methods. The first one is applying several different cleaning procedures, including de-ionized water rinsing or in-situ exposure to H_2, O_2 or SF_6 plasmas. Very stable magnetic properties were achieved over a period of ~6 months except O_2 plasma treated structures, with no evidence of corrosion, provided chlorinated etch residues were removed by post-etch cleaning. The second method is using non-corrosive gas chemistries such as CO/NH_3 or CO_2/NH_3. There is a small chemical contribution to the etch mechanism (i.e. formation of metal carbonyls) as determined by a comparison with Ar and N_2 physical sputtering. The discharge should be NH_3-rich to achieve the highest etch rates.

Several different mask materials were investigated, including photoresist, thermal oxide and deposited oxide. Photoresist etches very rapidly in CO/NH_3 and use of a hard mask is necessary to achieve pattern transfer. Due to its physically dominated nature, the CO/NH_3 chemistry appears suited to shallow etch depth ($\leq 0.5\mu m$) applications, but mask erosion leads to sloped feature sidewalls for deeper features.

CHAPTER 1
INTRODUCTION

Ferromagnetic thin films and multilayers have been researched intensively in recent years for application in various magnetic recording and nonvolatile memory devices.[1] Interest in these materials has increased dramatically since the discovery of giant magnetoresistance (GMR) in multilayers comprised of alternating ultrathin (10 to 50Å) ferromagnetic/noble metal layers. Briefly, the GMR effect can be understood in terms of spin-dependent scattering of conduction electrons at ferromagnetic/nonmagnetic interfaces. Conduction electrons with a spin direction parallel to a material's magnetic orientation move freely, providing low resistance. Conversely, conduction electrons with spin direction opposite to the materials magnetic orientation are hampered by more frequent collisions with atoms in the material, producing higher resistance.

In computer and data processing systems the main form of data storage and retrieval is based on magnetic recording systems, either magnetic disks or tape drives.[2-12] Information is written and stored as magnetization patterns on a recording media, and can be transferred back and forth using a magnetic sense head. In addition Magnetic Random Access Memories (MRAM) are used for storage and processing of very high bit densities. These devices offer the advantage over semiconductor memories of being radiation-hard, high storage densities, fast access time, and infinitely rewritable. Finally there are magnetic sensors, transducers and actuators which are used in automobiles, aircraft,

hydraulic equipment and defense applications (mine detection, perimeter defense).[1,9] In all of these structures there is a need to pattern the magnetic layers,[17] generally thin films of materials such as NiFe, NiFeCo, which are often incorporated into multilayers comprising magnetic and non-magnetic materials.

The fabrication of read/write heads and other magnetic storage elements requires methods for producing sub-micron features in multi-layer structures involving NiFe and NiFeCo.[1,13-17] Due to the relative involatility of the etch products of these materials in conventional plasma reactors, virtually all of the patterning is performed using ion beam etching or lift-off processes.[17-20] Both of these methods have drawbacks for producing very small features-ion beam etching has poor selectivity with respect to mask materials and can produce redeposition of the sputtered materials onto the feature sidewalls that degrades the magnetic performance of the devices, [18,19] while lift-off processes typically suffer from poor yield relative to direct etch removal methods.

In a typical reactive plasma process, exposure of NiFe and NiFeCo to chlorine or other associated feed gases produces a reaction or selvedge layer consisting of involatile etch products (i.e. $NiCl_X$, $FeCl_X$, $CoCl_X$ species).[18-22] Since these do not leave the surface and their atomic volumes are typically larger than those of the elements they are formed from, there is actually net deposition, rather than etching. There are basically two methods to enhance desorption of the etch products. The first is to heat the sample during plasma exposure to increase etch product volatility, but typically temperatures above 300°C are required,[18] and this exceeds the thermal "comfort-zone" of most magnetic multilayer structures. The second is to employ a high ion flux in conjunction with the

reactive chlorine neutral flux incident on the sample. The ion energy, however, must be kept low under these conditions to avoid mask degradation and loss of etch selectivity. The etch rates are a strong function of ion flux, ion energy and plasma gas composition, all of which may be interpreted in terms of balancing formation of chloride etch products with concurrent ion-assisted desorption of these products. Thus, the role of ion bombardment is critical in this mechanism. Alternative plasma chemistries including bromine or iodine containing plasmas were also examined under high density plasma conditions. The inter-halogens ICl and IBr have been found to dissociated readily in high density plasma sources, producing high concentrations of reactive species.

However one concern with this process is the effect of residual chlorine or chlorinated etch residues remaining on the sidewalls of etched features. We report on the effectiveness of several different in-situ or ex-situ cleaning processes after Cl_2/Ar high density plasma etching of GMR elements. We find that Inductively Coupled Plasma (ICP) etching does not degrade the magnetic performance of single or multilayer structures, and subsequent water rinsing or in-situ H_2 or SF_6 plasma cleaning is efficient in preventing corrosion.

Another method for preventing corrosion is applying non-corrosive gas chemistries such as CO/NH_3 or CO_2/NH_3. Nakatani[23] reported use of a non-corrosive CO/NH_3 plasma chemistry for NiFe, in which the etch products are expected to be carbonyls (e.g. $Fe(CO)_5$). The resultant etch rates were $\leq 300 Å \cdot min^{-1}$ for $Ni_{0.8}Fe_{0.2}$, a factor of about three higher than purely physical Ar^+ sputtering under the same conditions. The reactor employed was non-commercial, and might be classified as a magnetron-type,

medium ion density system. We report on a parametric investigation of CO/NH_3 etching of NiFe, NiFeCo and related thin film materials using an Inductively Coupled Plasma (ICP) reactor. We find maximum etch rates for NiFe and NiFeCo in the range 350-400Å·min^{-1}, with the rates being a strong function of $CO:NH_3$ ratio, source and rf chuck power and pressure. We also compared use of CO_2 to replace CO, though this does not appear to offer any advantage in etch rates.

In this dissertation, a comparison is given of high density plasma reactors such as ECR (Electron Cyclotron Resonance) and ICP (Inductively Coupled Plasma) based on either corrosive gas chemistries (Cl_2, IBr, ICl) or non-corrosive gas chemistries (CO/NH_3, CO_2/NH_3) will be described for the etching of NiFe, NiFeCo and other elements in magnetic multilayers. The influence of post-etch cleaning procedures on magnetic properties is also examined. Finally, the selectivity for etching the magnetic materials over common mask materials (photoresist, SiO_2) was measured over a broad range of conditions.

CHAPTER 2
MAGNETIC DEVICES

2.1. The Theory of GMR

In any material, some conduction electrons will be oriented with "up" spins, and some will be oriented with "down" spins. The material can be viewed as having two independent conduction channels, one for each electron spin orientation. The measured current will be the sum of these channels:

$$j = \sum_{s} j_s (s = \uparrow, \downarrow) \qquad (1)$$

In a non-magnetic material, these two currents are equal. In a magnetic material, such as Fe or Co, the two currents are different: interaction of a conduction channel with its surroundings will be spin-dependent. First, the conduction electron energy bands will be different for majority spin electrons (spin parallel to the magnetization). Second, minority and majority spin electrons will have different scattering potentials when they encounter impurities and interfaces. Thus, in a bulk ferromagnetic material, the resistivity of the majority spin channel ($\rho\uparrow$) is typically different from the minority spin channel ($\rho\downarrow$).[24,25]

In a multilayer structure where the layers are antiparallel, however, the up conduction channel will be scattered as majority spin electrons in one layer and as

minority spin electrons in the next layer, and vice versa. For this reason, the net resistivities of two channels will be the same, and approximately equal to the average resistivity of the two channels in the bulk:

$$\rho_{\uparrow} = a + b$$

$$\rho_{\downarrow} = a - b \qquad (2)$$

$$\overline{\rho} \cong \frac{1}{2}(\rho_{\uparrow} + \rho_{\downarrow}) = a$$

Conductivities (σ) of the two channels (σ_1, σ_2) add in parallel and the resistivity is the reciprocal of the conductivity. So:

$$\rho_{tot} = \frac{1}{\sigma_1 + \sigma_2}$$

$$= \frac{\rho_1 \rho_2}{\rho_1 + \rho_2} \qquad (3)$$

In the absence of an applied field, $\rho_1=\rho_2=\overline{\rho}$, and the total resistivity will be

$$\rho_0 = \frac{1}{2}\overline{\rho} = \frac{1}{2}a \qquad (4)$$

At the saturation field, on the other hand, $\rho_1=\rho\uparrow$ and $\rho_2=\rho\downarrow$. The layers will be oriented in parallel:

$$\rho_{sat} = \frac{\rho_\uparrow \rho_\downarrow}{\rho_\uparrow + \rho_\downarrow}$$

$$= \frac{a^2 - b^2}{2a} \qquad (5)$$

Clearly,

$$\rho_{sat} < \rho_0 \qquad (6)$$

In other words, an applied magnetic field (for instance, a field stored in magnetic media) "short circuits" the magnetic layers, reducing the total resistivity. This short circuit is observed as the GMR effect.

2.2. Basic Mechanism of GMR

Giant magnetoresistance is largely caused by a quantum effect called spin-dependent scattering, which results from the fact that the spin of an electron can point either up or down. Electrical resistance is caused by the scattering of electrons, but magnetic materials scatter spin-up and spin-down electrons differently (Figure 2-1).[26]

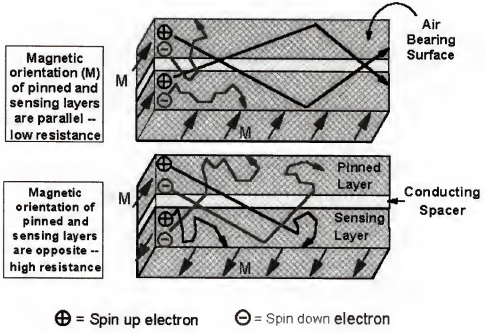

Figure 2-1. The Giant Magnetoresistance effect is due to the large difference in electrical resistance between two magnetic states of a metallic multilayer film.

Given a difference in resistivity between spin-up and spin-down electrons, the low resistance of the multilayer is generated when conduction electrons with a spin direction parallel to a material's magnetic orientation move freely. Conversely the higher resistance can be produced when conduction electrons with spin direction opposite to the material's magnetic orientation are hampered by more frequent collisions with atoms in the material.

A structure consisting of two magnetic layers are separated by a non-magnetic spacer layer. If the layers are magnetized in the same direction, both will scatter electrons in the same way and the structure will have almost the same resistance as the bulk material. However, if the layers are magnetized in opposite directions, one layer will mainly scatter spin-up electrons, while the other will scatter spin-down electrons. The overall resistance will increase.

The key point is that only a weak magnetic field is needed to change the orientation of the magnetic fields in the layers. By using a strong antiferromagnet to keep the orientation in one of the layers constant, changes in resistance can be linked to the magnetic state of the other layer.

There are two significant advantages of GMR over competing devices. First, the large resistance change yields a strong signal, and second, the technology is compatible with integrated circuit technology, so that GMR devices can be included as part of a chip package to make smaller, faster, less expensive sensors and memory chips.

2.3. GMR Read Heads

In the past couple of years, production of read heads for hard-disk drives has been largely converted from thin-file inductive heads to magnetoresistance heads using thin-film 80:20 nickel/iron magnetoresistors. This conversion was needed in order to get larger signals from smaller storage bits and keep pace with improvements in hard drives.

A read head detects a transition in magnetization stored in the disk as the head passes over it. The magnetic field produced by the transition is either up (head-to-head magnetization transition) or down (tail-to-tail magnetization transition).

The GMR read head uses a feature called a spin valve, which is etched into a material whose edge is oriented along the direction of the disk surface. Spin valve material normally composes of four thin films: a sensing layer, a conducting spacer, a pinned layer, and an exchange layer. The first three films are very thin, allowing conduction electrons to frequently move back and forth between the sensing and pinned layers via the conducting spacer (Figure 2-2).[26] The magnetic orientation of the pinned layer is fixed and held in place by the adjacent exchange layer, while the magnetic orientation of sensing layer changes in response to the magnetic field from the disk. A change in the magnetic orientation of the sensing layer will cause a change in the resistance of the combined sensing and pinned layers.

In the GMR read head, the magnetization of the pinned spin-valve layer is directed vertical to the disk surface, and the soft layer lies parallel to the surface in the absence of a field from the disk. Up and down magnetic field, which create smaller or larger resistance in the spin valve are generated by stored magnetic data on a rotating disk.

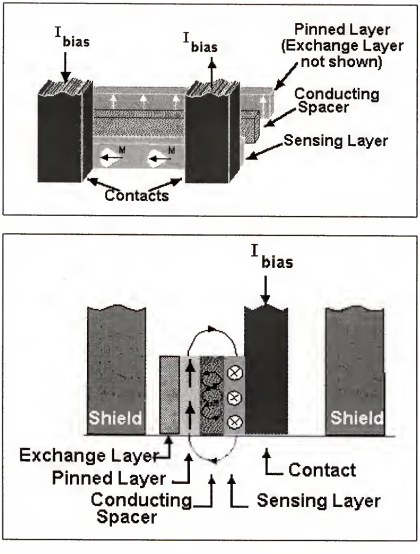

Figure 2-2. Structure and operation principle of GMR head.

2.4. Magnetic Random Access Memory

Nonvolatility the ability to store data when electricity is off is a much desired memory property in applications where data retention is critical. Semiconductor nonvolatile random access memory technologies, such as electrically erasable programmable read-only memory (EEPROM) and flash memory, suffer from slow write times and wear out after data are stored more than 1 million times. Memory that uses magnetic materials can have fast write times and can store data indefinitely.

Working memory systems using these magnetic RAM (MRAM) chips have used for space and missile application in which resistance to radiation damage is critical. Nonvolatility and radiation hardness are important for space missions, and magnet storage is intrinsically radiation-hard. Recently, GMR materials have been used to make MRAMs with faster read access times.

With proper design of the areal geometry and the right thickness of magnetic films, submicrometer-size MRAM cells (single memory bits) have been made to operate like a spin valve, and they have been called "pseudo spin valve" devices. They promise very high density, high speed and nonvolatile memory applications.

A newer high-mangetosistive innovation, called a spin-dependent tunneling (SDT) device, or magnetic tunnel junction (MTJ), uses tunneling current through a thin dielectric between two ferromagnetic films. STD devices work in a similar way to GMR devices. When two magnetic layers are magnetized in the same direction, the tunneling current is generally higher than when the two magnetic devices are magnetized in opposite directions.

CHAPTER 3
LITERATURE REVIEW OF PLASMA ETCHING PROCESSES

3.1. The Transition from Wet Etching to Dry Etching

Etch processes may be classified by their rate, selectivity, uniformity, directionality (isotropy or anisotropy), surface quality, and reproducibility. All etching processes involve three basic events: (1) movement of the etching species to the surface to be etched, (2) chemical reaction to form a compound that is soluble in the surrounding medium, and (3) movement of the by-products away from the etched region, allowing fresh etchant to reach the surface. Both (1) and (3) usually are referred to as diffusion, although convection may be present. The slowest of these processes primarily determines the etch rate, which may be diffusion or chemical-reaction limited. There are two different etching methods by using two quite different media: liquid chemicals (wet etching) and reactive gas plasmas (dry etching). Wet etching is performed by immersing the wafers in an appropriate solution or by spraying the wafer with the etchant solution.[27] Wet-chemical etching is superior to dry etching in terms of effectiveness, simplicity, low cost, low damage to the wafer, high selectivity and high throughput. However, the main limitations of wet etching include its isotropic nature which results in roughly equal removal of material in all directions, making it incapable of patterning sub-micron features, and the need for disposal of large amounts of corrosive and toxic materials. As the requirements developed for increasing circuit density and narrower line-width in the manufacture of VLSI (very large-scale integrated circuit)/ULSI (ultra large-scale integrated circuit) devices, it became necessary to have new

etching methods to replace the wet etching. Dry etching methods became favorable etching processes for integrated circuit manufacture. Plasma-driven chemical reactions and /or energetic ion beams are used to remove materials in dry etching system. The most significant advantage of dry over wet etching is that it provides higher resolution potential by overcoming the problem of isotropy. Other benefits are the reduced chemical hazard and waste treatment problems, and the ease of process automation and tool clustering.

3.2. The Ultimate Goals of a Dry Etch Process

The success of a etch process must be measured by the nine parameters listed below. The greatest challenge is that each parameter can usually only be optimized at the expense of at least one of the others.

(1) Critical dimension uniformity

Uniformity across the wafer-including densely populated areas and large open spaces, and within high aspect ratio features-is critical to maintain consistent device performance. Aspect ratio dependent etching also known as "micro-loading" is a common non-uniform problem.

(2) Selectivity

Defined as the ratio of the etch rate of one material versus that of another, the selectivity of the material being etched to the overlying masking layer (typically photoresist) is usually of the most concern, since this impact critical dimension and profile control, and the thickness of resist required (thinner photoresist is required to adequately resolve smaller feature sizes, so selectivity must increase as geometry

shrinks). Also of concern is the selectivity to the underlying material upon which the etch stops. Different selectivity specifications may be given for edges and flat areas, since edges tend to etch faster.

(3) Etch rate

High etch rate is needed to keep the throughput of the system or process module high (usually measured in Å/min). There is usually a tradeoff between etch rate and other parameters, such as selectivity and damage.

(4) Etch profile control

It's usually desirable to have an anisotropic profile, that is one where the etched feature edges are close to vertical, to maximize packing density on the chip. But it's also desirable to have a flare out at the top of the feature to enable good step coverage in subsequent deposition steps.

(5) Low damage

Damage is an obvious concern. The high energy of the plasma can create currents on the wafer surface that cause electrical damage and energetic ions can cause mechanical damage to the films' crystalline structure.

(6) Residue

Residue which coats the interior of the etch chamber is a difficult problem to avoid. In addition to requiring more frequent cleaning, residue is also a source of contamination. The most significant factors in controlling residue are temperature, bottom rf power, backside cooling and process pressure.

(7) Corrosion

Corrosion is mainly a problem in metal etch. Upon exposure to water vapor (i.e. air), chlorine will immediately attack metals. Integrated post-etch treatments help eliminate this problem.

(8) Particle control

Particle control is another critical measurement of etch system performance. Today, fewer than 0.05 particles/cm^2 that are >0.35μm in size are required.

(9) Sidewall passivation

Sidewall passivation is important both during and after the etch. Carbon from the photoresist mask typically combines with etching gases and etch byproducts to form a polymer-like material on the sidewall of the feature. This is usually a requirement in creating anisotropic profiles. The biggest challenge is that after the etch, this polymer must be removed.

3.3. Basic Mechanism of the Etch Process

The optimization of etch of these parameters–uniformity, selectivity, etch rate, profile control, damage, and residue control–requires an understanding and fine-tuning of the two very different mechanisms through which etching occurs.

As shown in Figure 3-1, one mechanism is purely chemical. Reactive species generated in plasma react with the wafer surface and create volatile etch products that swept away. By careful selection of the gases that are flowed into the plasma (typically chlorine and /or fluorine containing gases), it's possible to achieve very high selectivity through this

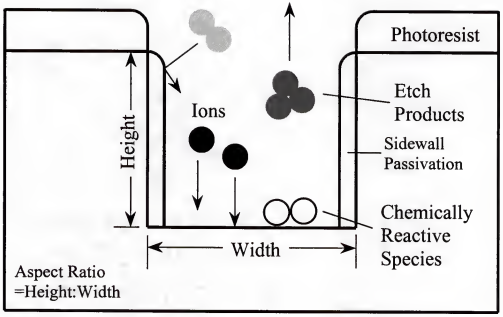

Figure 3-1. Schematic of plasma etching: etching occurs because of two etch mechanisms: chemical reaction and ion bombardment.

process. However, since films tend to etch in all directions at once, the result is an isotropic etch.

The other mechanism is purely physical. Energetic ions crossing the sheath transfer large amounts of energy and momentum to the substrate. The force of these ions can be strong enough to physically remove material. At low pressure where the mean free path is long, the ejected sputtered material can cross the reactor vessel and reach opposing walls. The main benefit of this etch mechanism is that it provides some directionality to the etch, making it possible to achieve highly anisotropic profiles. However, it is the least selective mechanism and also suffers from the disadvantages of low etch rate, damage and trenching.[28]

(1) Sputtering

In sputtering, impinging particles (usually positive ions accelerated across the sheath) strike the surface with high kinetic energy. Some of the energy is transferred to surface atoms which then are ejected, leading to a net removal of material. This process is distinguished from other etching mechanisms in that the interaction is mechanical. It is sensitive to the magnitude of bonding forces and structure of a surface, rather than its chemical nature and quite different materials can sputter at similar rates. In a way this is symptomatic of using ion bombardment with energy far higher than the surface binding energy.

(2) Chemical etching

Chemical etching comes about when active species from the gas phase encounter a surface and react with it to form a volatile product. Product volatility is necessary for chemical etching since involatile products would coat the surface and protect it from

further attack. In this type of the plasma reactor converts the feed into reactive chemical species, which are usually free radicals. There is usually no directionality and the etching can be specific (high selectivity) since it its governed by the relative chemical affinities between the etchant species and exposed materials. Because of this lack of directionality, chemical etching is commonly called isotropic etching

(3) Energy-driven ion-enhanced etching

There is usually little of no etching when the substrate surface is exposed to neutral chemical species alone in the absence of ion bombardment. Impinging ions damage the substrate material by virtue of their impact energy, and thereby render the solid substrate more reactive toward incident neutral radicals.

(4) Inhibitor-driven ion-assisted etching

Inhibitor-protected sidewall ion-enhanced etching differs from energy-driven ion-enhanced etching is that the chemical etching reaction in spontaneous, even without ion bombardment. Neutral etchant species from the plasma spontaneously gasify the substrate, and ions play a role by interaction with another component-a 'protective' inhibitor film. The role of ions in the surface-inhibitor mechanism is to clear the inhibitor from horizontal surfaces that are bombarded by the flux of ions impinging in the vertical direction. The protective film is not removed from the vertical walls of masked features because these surfaces only intercept those few ions that are scattered as they cross the sheath. This protective film may originate from involatile etching products or from film-forming precursors that adsorb during the etching process.

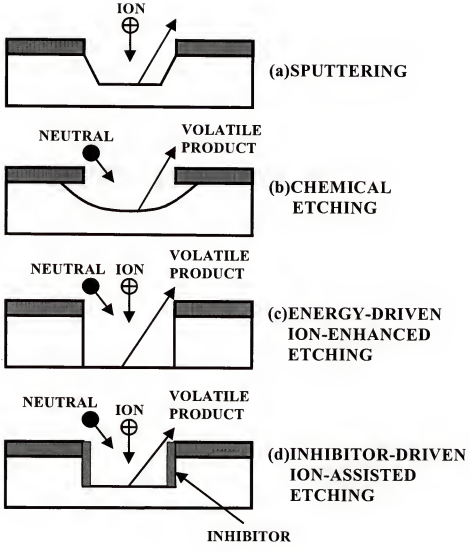

Figure 3-2. The four basic mechanisms of plasma etching:
(a) sputtering
(b) purely chemical etching
(c) energy-driven ion-enhanced etching
(d) Inhibitor-driven ion-assisted etching

3.4. Dry Etching Techniques

(1) Plasma etching

A wafer is exposed to a reactive gas such as chlorine which is in some cases dissociated in a plasma to create highly reactive atoms. Etching is isotropic or crystallographic, and temperature and reactant flux are used to adjust etch character. During the purely chemical etching process, three steps occur: adsorption of the necessary species on the materials surface, chemical reaction, and desorption of the products. The advantage of the technique is rapid etch rates, but the drawbacks are isotropy, a tendency for strong loading effects, and release of heat.

(2) Ion Beam Etching

Ion beam etching (ion milling) uses a broad-area ion beam composed of a nonreactive gas such as Ar with high ion energy. This technique only relies on physical sputtering. The uniform ion beam bombards a wafer to cause etching. Since ion beam etching is very anisotropic and the wafer is not exposed to plasma, it is well suited for etching of certain patterns.

A major problem with ion beam etching is that the etch rate is very low because of the nature of physical sputtering, and it is also recognized that the etch rate of ion milling is very much dependent upon the incidence angle. It typically peaks at between 30° and 50°, and becomes very small when angle is larger than 80°. There are a number of factors that limit the application of ion beam etching. First of all, etch products, usually nonvolatile, can redeposit on the wafers, especially onto the sidewalls of etch mask that degrades the magnetic performance of the devices. When

the film plane is normal to the ion beam, the etch rate of the sidewalls is very small since the incidence angle there is close to 90°. As a result, after the etch mask is removed, undesired fence and trenches are often left on the edges of the etched patterns.

(3) Reactive Ion Etching

Reactive ion etching uses radiofrequency power to maintain a plasma. Applied rf power makes electrons accelerate in the sheath region changing direction upward and downward. The accelerated electrons can lose a large fraction of their kinetic energy through dissociative collisions with molecules and atoms. Because electrons are light and have high energy, they diffuse fastest, leaving an excess of positive charge and a plasma potential that is positive relative to the electrode. Since charged particles are most abundant in the central glow of the plasma, most of the potential drop appears across the sheath. Positive ions are accelerated through the sheath and strike the samples, giving rise to a physical etch component. In addition, ion flux is coupled with ion energy. High plasma densities and ion fluxes are gained at the expense of extremely high applied voltages and damage levels.

3.5. High-Density Plasma Reactor

Increasingly, the limitation of traditional plasma etch technologies-which has resulted in the trend to high density plasma sources-is primarily one of process pressure. In the pressure regime of a few hundred millitorr where it's relatively straightforward to create

a plasma, it becomes difficult to get etchant in and reaction byproducts out of openings that are smaller than about 0.25μm. The problem is more sever with higher aspect ratio.

The solution is to go to lower pressures, where the mean free path lengths of gas molecules and ions are longer, which reduces scattering collisions that can cause loss of profile control

However, this is not as simple as it may seem since it requires a switch to a different type of plasma source-a so-called high density source-that is capable of generating enough ions to achieve acceptable etch rates at reduced pressure. High density sources are designed to more efficiently couple input power with the plasma, resulting in greater dissociation of etch species.

Although a wide variety of high density source types have been developed, they generally fall into one of three categories: electron cyclotron resonance (ECR), helicon resonance or inductively coupled plasma (ICP) type sources. All three are in use on production equipment. The main difference is that ECR and helicon sources employ an external magnetic field to shape and contain the plasma, while ICP sources do not.[29]

(1) Electron Cyclotron Resonance (ECR) Plasma

Various methods have been developed for reducing ion energies in the discharge which trying to maintain anisotropic etching. One of the methods involves the addition of magnetic fields configured to reduce electron loss from the plasma and the sample. This method of magnetically enhancing the discharge is called ECR plasma etching. In ECR discharges, free electrons in the plasma are forced to orbit about magnetic field lines while absorbing microwave energy. At the cyclotron resonance

condition, outer shell electrons from gas molecules in the discharge may also be liberated, leading to a very high degree of ionization in the plasma. Since the motion of the electrons is constrained by the external magnetic field, fewer are lost by collisions with the reactor walls than conventional RIE, and therefore the plasma potential relative to ground is much lower. The resultant energies of an ion reaching the sample to be etched are typically ≤15eV. ECR etching should lead to much lower levels of damage than conventional RIE processes. ECR sources operate at the relatively high ion density of 10^{11}~10^{12}cm^{-3} compared with RIE tools (~10^{9}cm^{-3}). ECR tools can also provide independent control of the ion energy and ion flux. Ion energy is controlled by rf or dc biasing of the substrate holder while control of the ion and neutral flux is achieved by varying the microwave power and neutral gas pressure. In addition, ECR discharges are capable of low pressure operation due to its efficient dissociation of gases from the discharge.

(2) Inductively Coupled Plasma (ICP)

Another high density plasma, ICP, has become popular because of disadvantages of the ECR technology. ECR suffers from difficulties in uniformity. The power supply may also limit the scaling of the ECR approach without the development of higher power magnetrons. The primary disadvantages of the ECR technology are the limits due to a commercially available, automatic-tuning microwave power supply, and the physical limits of the magnets required to create a uniform magnetized plasma. ECR tools appear difficult to scale to process wafers larger than 200mm.

In the ICP geometry, a rf coil encircles the chamber. The important features of this coil are that it carries rf current and generates a magnetic field in the upward and downward directions. The time rate of change of the individual magnetic field generates an electric field. Acceleration of the electrons is determined by the magnitude of the electric field, confining them in a circular motion. The plasma, first formed in the shape of a ring following the path of electrons, will diffuse to the center of the chamber and then downward toward the sample. The electrons, in circular path, will have only a small chance to be lost to the chamber walls, resulting in low dc self bias. Ion energy, separated from the ion flux, can be controlled by applying another rf source at the chuck. Unlike ECR plasma sources, there is no resonance between electron motion and the frequency of the driving fields in ICP sources. Therefore, ICP sources have advantages over ECR sources, including easier tuning, scaling up and lower cost.

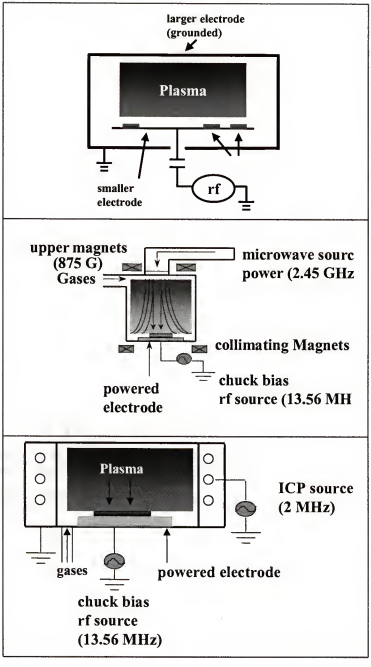

Figure 3-3. Schematics of typical Reactive Ion Etcher (RIE, top), Electron Cyclotron Resonance (ECR, center) and Inductively Coupled Plasma (ICP, bottom).

CHAPTER 4
HIGH-DENSITY PLASMA ETCHING FOR PATTERNING OF NiFe AND NiFeCo

4.1. Introduction

Magnetic materials such as NiFeCo and antiferromagnetically coupled Fe/Cr or Co/Cu mutilayers are widely used in the data storage industry for non-volatile memories, magnetic sensors and microactuators.[1,10] Other materials such as TaN and CrSi can be also used as oxidation or contact barriers, respectively, in Magneto-Resistive Random Access Memory (MRAM) stacks. However, a problem for future development is that there has been little success obtaining high rate dry etching processes for magnetic materials, critically blocking the ability to batch-fabricate submicron magnetic devices.[30-32] Generally, magnetic materials and related metals are inert in conventional dry etch processes like reactive ion etching (RIE).[28,30] Simple Ar^+ ion milling is undesirable for small geometry pattern transfer because of redeposition on the sidewalls that degrades the magnetic performance of the devices. Magnetic structures have been finding a dominant role as nonvolatile storage devices for computers, audio, video, etc. A representative magnetic device is a thin film magnetic read/write head. A typical recording head currently has a ~2μm track width. This can be achieved by conventional ion beam etching processes. However, submicron track width magnetic heads should be necessary to accomplish disk drives with recording density of ≥10Gbit/in^2, and in this situation pattern transfer processes with some degree of chemical etching are necessary.

In this chapter we compare the performance of two different high density plasma reactor types, namely ECR and Inductively Coupled Plasma (ICP), for etching of NiFe, NiFeCo and two materials used as oxidation or contact barriers in multilayer magnetic structures, namely TaN and CrSi. We have investigated a wide range of plasma chemistries, and find that only Cl_2/Ar produces a chemical enhancement in etch rate of the NiFe and NiFeCo. Post-etch cleaning processes using H_2 plasmas were also investigated, and the selectivity for etching the magnetic materials with respect to various masks was measured. Under most conditions it is necessary to employ dielectric layers as mask materials, since photoresist is degraded under the high ion flux present in ECR and ICP reactors.

4.2. Materials and Experimental Procedure

DC magnetron sputtering was used to deposit layers of $Ni_{0.8}Fe_{0.2}$ and $Ni_{0.8}Fe_{0.13}Co_{0.07}$ approximately 5,000Å thick on Si samples. In some case, the samples were then deposited with 3,000Å of SiO_2 or SiN_X, which were subsequently employed as masks. All samples were lithographically patterned with photoresist and in the case of those with the SiO_2 or SiN_X, the pattern was transferred into these dielectrics by SF_6/Ar ECR dry etching (2mTorr, 150W rf, 300W ECR source power). The end result was that we were able to compare photoresist, SiO_2 and SiN_X as mask materials for the subsequent etching of the magnetic materials.

Two different plasma reactors were used in these experiments. The first was a Plasma Therm 790 ICP system, in which the sample sits in an 8″ ϕ, rf (13.56MHz)

biased, He backside-cooled electrode. The rf power was received from 50-450W, and this controls the dc self-bias in the electrode at any given source power (typical range -40V to -205V at 500W source power). The plasma is generated by application of 2MHz rf power (0-1500W) to the ICP source, using a 3-turn planar antenna geometry which is closely coupled (plasma-sample distance ~4cm) to the sample electrode. The process pressure was generally held constant at 2mTorr, with typical total gas loads of 15 standard cubic centimeters per minute (sccm). The second reactor is a Plasma Therm SLR 770 ECR system, with a 4" ϕ sample electrode also biased with 13.56MHz rf power (50-250W, corresponding to self-biases of -70V to -310V at 500W source power) and He backside-cooled. The plasma is generated in a 2.45GHz (0-1000W) ASTEX 4400 low profile ECR source, at a process pressure typically of 1.5mTorr.

Etch rates were measured by stylus profilometry of the features after removal of the mask materials, while feature anisotropy was examined by scanning electron microscopy (SEM) and near-surface atomic composition by auger electron spectroscopy (AES). The magnetic properties before and etching were determined by SQUID magnetometry at 4.2K.

4.3. Electron Cyclotron Resonance Plasma Etching

A preliminary method for predicting whether or not a material can be etched in a particular plasma chemistry is to look at the vapor pressure of potential etch products. Table 1 shows that the boiling points of the possible etch products of the samples in this study in halogen plasma chemistries are very high. This means that volatilities of etch

products are very low.[33] We cannot expect acceptable etch rates without some other form of desorption mechanism. There are two possibilities for enhancing desorption of the involatile components. The first one is by ion-assistance or sputtering. Conventional reactive ion etching employs high ion energy (≥200eV), but low ion density (~$10^9 cm^{-3}$).[34] These are not suitable conditions for removing nonvolatile etch products because one generally builds up a thick selvedge layer that prevents access of the reactive neutrals to the sample surface. The other possible approach is heating the sample during etching. This also has problems in terms of restrictions on the type of mask materials that can be employed and the anisotropy of etched features is degraded unless sidewall passivation techniques are used.

Figure 4-1 shows the etch rates of NiFeCo or a function of both microwave source power (top) and rf chuck power (bottom) for a number of different plasma chemistries in the ECR reactor. These chemistries represent all the main classes used for dry etching, namely Cl_2-, F_2-, Br_2- or CH_4/H_2- based gas mixtures. As seen in the top peak of the Figure, only Cl_2/Ar provides a faster rate than pure Ar alone, while the other chemistries (except BCl_3/Ar at high source powers where there is a high atomic Cl density) actually retard material removal. Similar results were obtained with NiFe, but the absolute rates were approximately a factor of 2 higher than for NiFeCo.[35] From the lower part of the figure, it is also obvious that there exists an ion energy threshold for the onset of etching, but that if the rf chuck power is increased too much, the etch rate decreases for Cl_2/Ar. This has been observed previously in ECR etching, and is usually ascribed to Cl species being removed from the surface before they can react to form the etch products.[36,37] The

Table 4-1. Boiling points of potential etch products

Products	Boiling point (°C)	Products	Boiling point (°C)
$TaCl_5$	239.35	$NiCl_2$	subl 973
$TaBr_5$	348.8	$NiBr_2$	subl
TaI_5	543	NiI_2	subl
TaF_5	299.5	NiF_2	1740
NCl_3	71	$FeCl_3$	316
NBr_3	.....	$FeCl_2$	1023
NI_3	subl vac	$FeBr_3$	.....
NF_3	-128.8	$FeBr_2$	934
$CrCl_4$	dec>600	FeF_3	726
$CrCl_3$	dec 1300	FeF_2	1837
$CrCl_2$	1300	$CoCl_3$	.....
$CrBr_3$	.....	$CoCl_2$	1049
$CrBr_2$	.....	$CoBr_2$	.....
CrI_3	vac 350	CoI_2	570
CrI_2	subl vac 800	CoF_3	.....
CrF_3	subl 1100	CoF_2	1739
CrF_2	>1300	SiF_4	-86
$SiCl_4$	57.65	Si_2F_6	-18.5
$SiBr_4$	154	SiH_4	-111.8
Si_2Br_6	240	Si_2H_6	-14.5
SiI_4	287.35	Si_3H_8	52.9

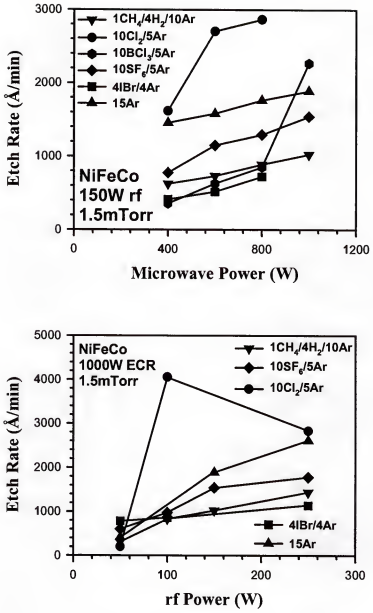

Figure 4-1. NiFeCo etch rates in different plasma chemistries at fixed rf chuck power (150W) and pressure (1.5mTorr) as a function of ECR microwave source power (top) or rf chuck power (bottom).

threshold rf power for initiation of etching in Cl_2/Ar corresponds to a dc self-bias of ~65V, while the etch rate maxima occurs at ~-120V.

Similar data is shown in Figure 4-2 for NiFe. There are several features to note in each plot. First, only Cl_2/Ar provides a clear etch rate enhancement over simple Ar sputtering and this rate is proportional to source power over the range of 400-1000W. We found from separate experiments that the etching is not limited by the supply of Cl_2 to the surface under these conditions, since increasing the ratio of Cl_2-to-Ar actually decreased the etch rate. Rather, the key feature is maintaining an argon ion-to-chlorine neutral ratio that allows a continues balance between formation of $NiCl_X$ and $FeCl_X$ products, and their efficient ion-assisted desorption. If the Ar-to-Cl_2 ratio is allowed to become too large, we revert to basically physical sputtering. Conversely, if the Cl_2 coverage density becomes too high (via discharge composition, pressure, or having too low an ion flux or energy), then the etching is quenched, and one may even have net deposition through formation of a chlorinated selvedge layer. The second feature of the data in Figure 4-2 is that SF_6/Ar or CH_4/H_2/Ar plasma chemistries produce etch rates lower than simple sputtering, indicating that the fluoride and methyl-adduct reaction products are not volatile, and actually shield the NiFe surface, reducing the sputter rate. Similarly, in a Cl_2/H_2 discharge, the NiFe etch rate is again lower than that of Ar sputtering. These are two possible contributions to this result-the light H_2^+ ions are inefficient in sputtering the nickel and iron chlorides and optical emission spectroscopy shows that the atomic Cl density is reduced in a Cl_2/H_2 discharge relative to Cl_2/Ar at the same conditions through recombination with atomic hydrogen. The similar dependencies of NiFe removal rate in Cl_2/Ar and pure Ar with microwave power indicates that the rate-limiting step with the former is still the

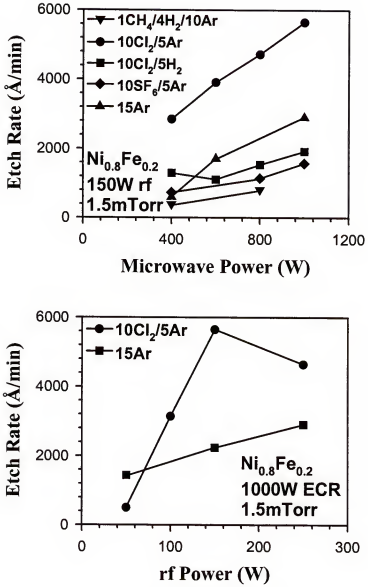

Figure 4-2. NiFe etch rates in different plasma chemistries at fixed rf chuck power (150W) and pressure (1.5mTorr) as a function of microwave source power (top) or rf chuck power (bottom).

desorption of the chloride etch products since the main effect of increasing source power is the associated increase in ion flux to the sample.

The data in the lower part of Figure 4-2 shows that there is a threshold ion energy (at constant ion flux) to efficiently remove the etch products. The NiFe rate increases rapidly with chuck power (or equivalently ion energy)[38] and is above sputter rate at a power of ~70W corresponding to a dc self-bias of -65V. Above a chick power of ~150W (dc self-bias -135), the etch rate decreases. This type of behavior is commonly observed in ECR etch processes, and is usually ascribed to the active etch species (Cl neutrals in this case) being removed by ion-assisted desorption before they have a chance to complete formation of the etch products.[34,37] We observed the same qualitative trends in etch rate of NiFeCo with both source and chuck power, with all rates being roughly 50%-80% lower than for NiFe.

Figure 4-3 shows AES surface scans of NiFeCo after a brief etch in 1.5mTorr, 150W rf chuck power discharges of $10Cl_2/5Ar$, with either 0 W ECR source power (top), which corresponds to conventional reactive ion etching (RIE), or with 1000W source power (center). In the former case, there is a large peak due to chlorine resides, consistent with formation of a thick (≥100Å) chlorinated selvedge or reaction layer that prevents further etching.[39] However with a high ion flux simultaneously incident with chlorine adsorption, the chlorinated etch products are removed as quickly as they form and a balance is maintained between product formation and product removal by ion-assisted desorption. This mechanism exposes a fresh surface for the process to occur all over again. Note in Figure 4-3 that the Ni - to - Cl ratio (in raw, uncorrected counts)

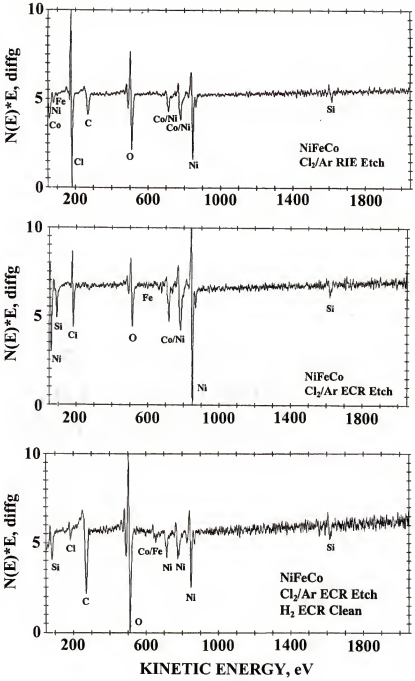

Figure 4-3. AES surface scans of NiFeCo after a brief etch in $10Cl_2/5Ar$, 1.5mTorr,150W rf chuck power discharges with either 0W ECR microwave source power (top) or 1000W microwave source power (middle). In the bottom case, the sample was also cleaned with an in-situ H_2 plasma for 10mins after etching with 1000W microwave source power.

decreases from ~0.5 for the RIE sample to ~2.5:1 for the ECR sample. Further exposure of the ECR etched sample to an in-situ H_2 plasma removes even more of the chlorinated residues, providing a Ni:Cl ratio of ~5.7:1 (Figure 4-3, bottom).

The presence of chlorine-related surface (and sidewall) residues is clearly of concern with respect to subsequent corrosion of the metal. In the current case we have investigated a number of in-situ post Cl_2-etch cleaning steps to remove these surface residues.[40] AES depth profiling of the ECR etched samples showed the Cl was restricted to ≤20Å from the immediate surface. The Cl concentration could be reduced to the sensitivity limit of AES (≤1 at. %) by a 3 minutes, 15mTorr H_2 plasma treatment at 1000W ECR source power with 0W rf chuck power. We expect that the chlorine residues are volatilized as HCl during exposure to the H_2 plasma. Note that we have only examined surface residues on the field between features and at this point not on the feature sidewalls where the initial residue thickness might be expected to be greater because of the absence of ion bombardment during the initial etch step.

SEM micrographs of features etched into 5000Å thick NiFe layers masked by 1500Å thick oxide are shown in Figure 4-4. The sidewalls are smooth and straight, and we have not seen any obvious visual effects of corrosion over a period of several months indicating there is not gross contamination of the sidewall with chlorine residues. Note that photoresist masks did not hold up well for microwave source powers above ~600W (Figure 4-5) because the high ion flux leads to significant preferential sputtering of H from the near surface and degrades the resist morphology and dimensional integrity.

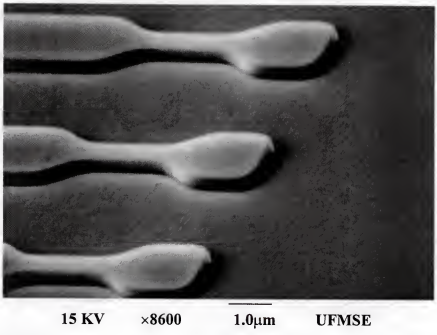

Figure 4-4. SEM micrograph of feature etched into NiFe layers using an ECR $10Cl_2/5Ar$ plasma (800W microwave source power, 150W rf power, 1.5mTorr). The oxide masks are still in place.

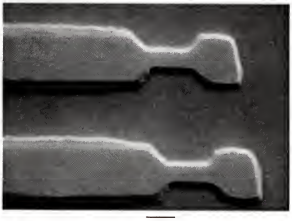

Figure 4-5. SEM micrographs of features etched into NiFe using a $10Cl_2/5Ar$, 150W rf, 2mTorr, 1000W ECR microwave source power discharge, with a photoresist mask (top), which has been subsequently removed (bottom).

Under these conditions, the oxide and nitride masks were stable and are better choice as masking materials.

Since the earlier AES data showed that there are still chlorinated surface residues remaining after etching, the question of post-etch corrosion of the magnetic materials is a very important one. We have found that a simple, fixed-time H_2 plasma in-situ clean may or may not be sufficient to prevent subsequent corrosion of the wafer upon removal from the etch reactor. For example, Figure 4-6 shows SEM micrographs of NiFe features etched in a "clean" ECR chamber (i.e. The first run with Cl_2/Ar after a prolonged set of runs with O_2 or SF_6). The samples were exposed for a set period of 10min. after the etching to a 10mTorr, 500W source power, -25V dc H_2 plasma, and then exposed to air ambient for 3 weeks. The sidewalls of the features show no evidence of corrosion. By sharp contrast features etched later in the same set of Cl_2/Ar runs (i.e. After the reactor chamber walls will be saturated with chloride residues), and then cleaned with the same type of H_2 plasma, showed extensive corrosion after just a 2 weeks exposure to air ambient (Figure 4-7). Clearly we must make sure the condition of the chamber walls is consistent if the H_2 plasma clean is to be consistently effective. To be sure of avoiding any corrosion, it will probably be necessary to employ post-etch wet chemical cleaning protocols, similar to that for Al etching in Si technology.[40,41]

The selectivity for etching NiFe and NiFeCo over the dielectrics in 150W chuck power, 10Cl_2/5Ar discharges is shown in Figure 4-8 as a function of microwave source power. For both magnetic materials, oxide provides higher selectivity than nitride, and the selectivities are higher relative for NiFe due to its higher etch rates compared to NiFeCo.

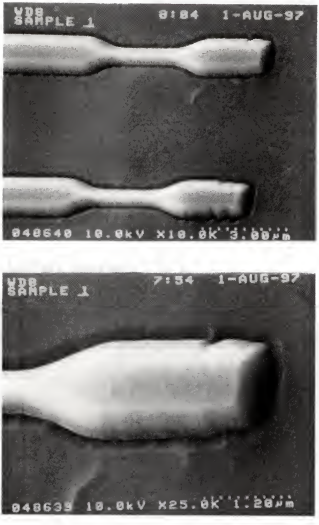

Figure 4-6. SEM micrographs of features etched into NiFe using $10Cl_2/5Ar$, 1.5mTorr, 150W rf chuck power, 1000W microwave source power discharges in an initially "clean" chamber (no previous Cl_2 plasma had been seen for a considerable period), followed by a 10min in-situ H_2 plasma clean. The samples were then exposed to air ambient for 3 weeks. The SiO_2 mask are still in place.

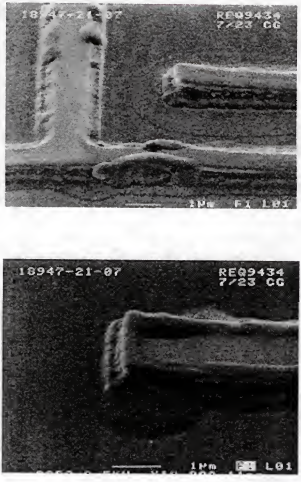

Figure 4-7. SEM micrographs of features etched into NiFe using the same conditions as Figure 4-6, but numerous Cl_2 plasma had been used prior to doing the etch and subsequent H_2 plasma clean. The samples were then exposed to air ambient for 2 weeks. The SiO_2 masks are still in place.

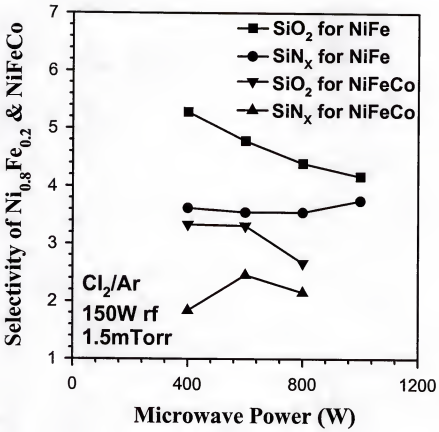

Figure 4-8. Etch selectivity of NiFe and NiFeCo over SiO_2 and SiN_X mask materials in $10Cl_2/5Ar$, 1.5mTorr, 150W rf chuck power discharges, as a function of ECR microwave source power.

4.4. Inductively Coupled Plasma Etching

4.4.1. Cl_2-based Plasma Chemistries

Figure 4-9 shows the etch rates of NiFe, NiFeCo, CrSi, and TaN in Cl_2/Ar discharges at fixed ICP source power (750W), dc self-bias (-100V) and pressure (2mTorr), as a function of percentage Cl_2 in the total gas flow. All of the materials show the same basic trend of going through an etch rate maximum at ~66% Cl_2. We see this type of behavior frequently for materials with relatively low volatility etch products.[42-43] At low Cl_2 flows, the etching is dominated by pure Ar sputtering, and is slow. As the Cl_2 percentage in the discharge increases, the etch rate rises rapidly, indicating the presence of a significant chemical component in the etch mechanism. Beyond a particular composition however (which is a function of pressure, ion flux and ion energy), the etch rate decreases again because the ion-to-neutral ratio becomes too low, allowing a chlorinated selvedge (reaction) layer to form on the surface. Note also that the peak etch rates are only around 700Å·min^{-1} for NiFe and NiFeCo, well below those we found previously for ECR etching. From other experiments we believe the ion flux is somewhat lower in our ICP tool,[43,44] and is capable of more controlled etching than the ECR reactor.

Similar data is shown in Figure 4-10 for the Cl_2/N_2 plasma chemistry. The same basic trends are evident as were seen with Cl_2/Ar, but the overall etch rates are lower, probably because N_2^+ and N^+ ions are less efficient at helping desorb the chloride etch products than are the heavier Ar^+ ions. Cl_2/N_2 discharges have previously been reported to produce more atomic chlorine neutrals than Cl_2/Ar,[44] but if that indeed is the case it does

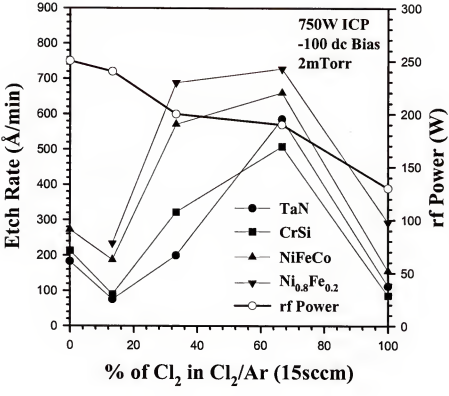

Figure 4-9. Etch rates of NiFe, NiFeCo, TaN and CrSi are function of plasma composition in ICP Cl_2/Ar discharges (750W source power, -100V dc self-bias, 2mTorr pressure).

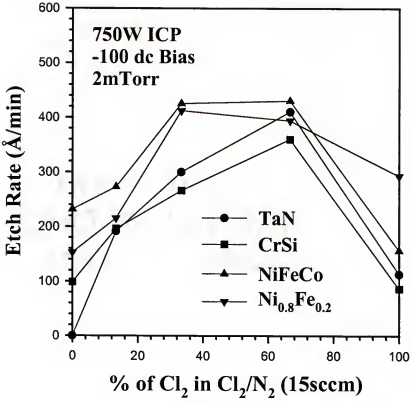

Figure 4-10. Etch rates of NiFe, NiFeCo, TaN and CrSi as a function of plasma composition in ICP Cl_2/N_2 discharges (750W source power, -100V dc self-bias, 2mTorr pressure).

not assist the etch rate in our case because product desorption is the limiting step, not chlorine supply.

Figure 4-11 comprises results for NiFeCo etching in the three different plasma chemistries investigated, namely Cl_2/Ar, Cl_2/N_2 and Cl_2/H_2, as a function of plasma composition. The results show quite clearly that in terms of etch rates, Ar addition produces the highest values, and this is most likely due to its better sputtering efficiencies.

The ICP source power basically controls the ion flux incident on the sample. Figure 4-12 shows the etch rates of the four materials at constant dc self-bias (rf power was examined as the source power was increased in order to keep the dc chuck bias at -80V), fixed plasma composition and pressure, as a function of source power. While the etch rates for TaN and CrSi increase almost linearly with ion flux, those for NiFe and NiFeCo go through maxima. This indicates for these latter materials that if the ion-to-neutral ratio becomes too high, chlorine is ejected from the surface by sputtering before it has a chance to react and form the chlorinated etch products.

The etch rates are also a strong function of ion energy, as seen in Figure 4-13, which shows their dependence on rf chuck power at constant source power (750W), pressure (2mTorr) and plasma composition ($10Cl_2/5Ar$). There tends to be some saturation in etch rates at the highest dc self-biases (the voltage through which ions from near the plasma sheath are accelerated to the sample position), which probably indicates again that the chlorine could be removed by sputtering before it has a chance to react with the surface if the ion energy becomes too high.

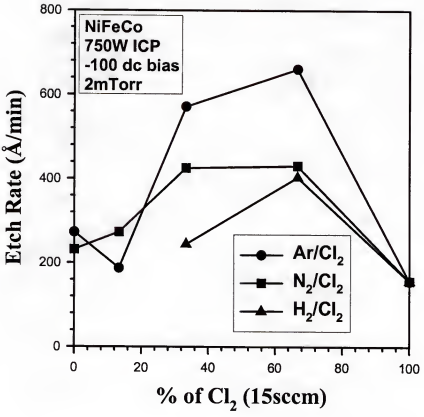

Figure 4-11. Etch rates of NiFeCo as a function of plasma composition in ICP Cl_2/Ar, Cl_2/N_2 or Cl_2/H_2 discharges (750W source power, -100V dc self-bias, 2mTorr pressure).

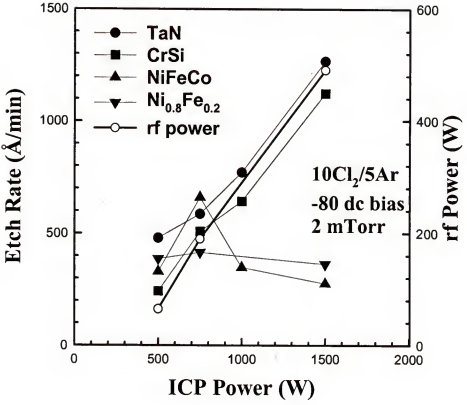

Figure 4-12. Etch rates of NiFe, NiFeCo, TaN and CrSi as a function of ICP source power in $10Cl_2/5Ar$, 2mTorr, -80V dc self-bias discharges.

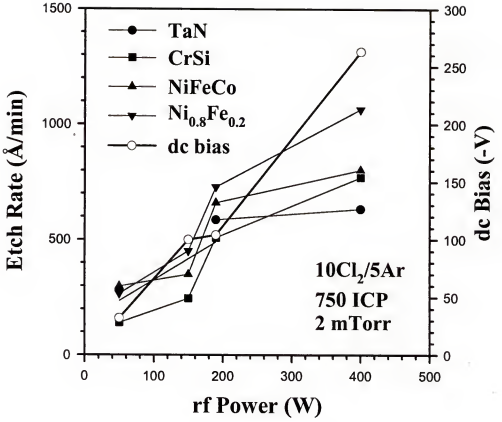

Figure 4-13. Etch rates of NiFe, NiFeCo, TaN and CrSi as a function of rf chuck power in $10Cl_2/5Ar$, 2mTorr, 750W source power discharges.

Further evidence that the ion-to-neutral ratio is the critical factor determining etch rates comes from the pressure dependence data shown in Figure 4-14. At fixed dc self-bias (-100V), source power (750W) and plasma composition ($10Cl_2/5Ar$), the etch rates fall monotonically with pressure. Note that the rf chuck power required to produce a self-bias of -100V dc also decreases in a similar fashion with increasing pressure, indicating that the ion density in the plasma is decreasing as pressure is increased. Under these conditions therefore, the chlorine coverage of the surface will increase and retard the etch rates because there is less ion flux to desorb the etch products.

Examples of the type of etch anisotropy and mask stability obtained in this type of etching are shown in the SEM micrographs of Figure 4-15. The micrograph at top shows feature etched into NiFe layers using on SiO_2 mask, which is still in place. The feature sidewalls are vertical and smooth. By contrast, photoresist does not retain its dimensional stability during exposure to the ICP discharge, as shown in the micrograph at the bottom of the figure. Typical selectivities of ~4-6 were obtained for etching NiFe over SiO_2 and SiN_X, similar to those for the ECR process reported earlier.[35]

The AES data contains the role of ion energy and flux in the etch mechanism. Figure 4-16 shows AES surface scans from NiFeCo after etching in $10Cl_2/5Ar$ discharges at two different rf chuck powers. The samples were exposed to atmosphere during transfer from the etch reactor to the AES analysis chamber, and this results in a native oxide and the presence of adventitious carbon. However, there is clearly more residual chlorine on the surface of the sample etched at lower rf chuck power, which is consistent with the notion that desorption of the chloride etch products is the limiting factor determining etch rate. There was a much lesser amount of chlorine residues observed on

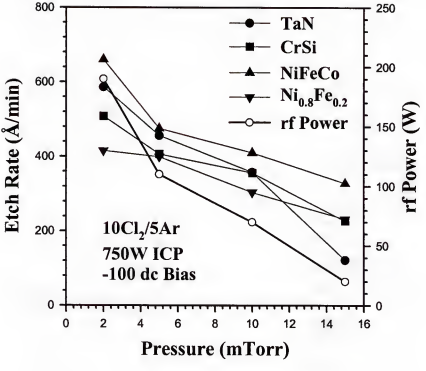

Figure 4-14. Etch rates of NiFe, NiFeCo, TaN and CrSi as a function of process pressure in $10Cl_2/5Ar$, -100V dc self-bias, 750W source power discharges.

Figure 4-15. SEM micrographs of features etched with NiFe using $10Cl_2/5Ar$, 2mTorr, -100V dc self-bias, 750W ICP source power discharges, using either a SiO_2 mask (top) or a photoresist mask (bottom), both of which are still in place.

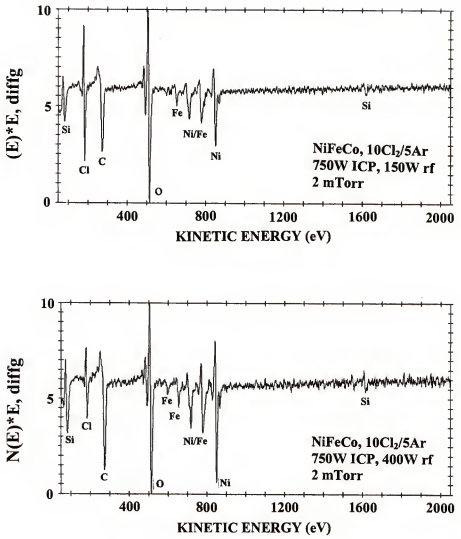

Figure 4-16. AES surface scans of NiFeCo after etching in $10Cl_2/5Ar$, 2mTorr, 750W source power discharges at either 150W (top) or 400W (bottom) rf chuck power.

the TaN and CrSi etched under the same conditions ($10Cl_2/5Ar$, 150W rf power, 750W source power, 2mTorr pressure), as shown in the AES surface scans of Figure 4-17. To remove these residues prior to opening the etch chamber, we have previously reported the use of in-situ H_2 plasma cleans,[35] which volatilize the chlorine as HCl. Our experience with this procedure is that it is quite effective in preventing post-etch corrosion of the magnetic materials, but that it is necessary to pay careful attention to the condition of the reactor chamber walls. Thus, if many Cl_2 plasma etch runs have been performed sequentially in the reactor, it is necessary to run the subsequent H_2 plasma for a much longer period than if only a few Cl_2 runs had been done.

4.4.2. Inter-Halogen Plasma Chemistries

While the Cl_2/Ar plasma chemistry operated under high density conditions produces effective etching of magnetic materials, there are other mixtures of interest. In particular, the inter-halogens ICl and IBr have been found to dissociate readily in high density plasma sources, producing high concentrations of reactive species.[45]

The influence of plasma composition on Ni, Fe, NiFe and NiFeCo etch rates in ICP ICl/Ar (top) and IBr/Ar (bottom) discharges at fixed source power (750W), rf chuck power (250W) and pressure (5mTorr) is shown in Figure 4-18. For the ICl/Ar plasma chemistry the rates for NiFe, NiFeCo and Ni initially increase as ICl is added, but then decrease beyond particular discharge compositions. This is consistent with a mechanism in which the adsorbed reactive neutral flux must be balanced with the ion-assisted removal of the resultant etch products.[46,47] Beyond the optimum discharge compositions, we believe there is blocking of the surface to ion bombardment by the high chlorine and

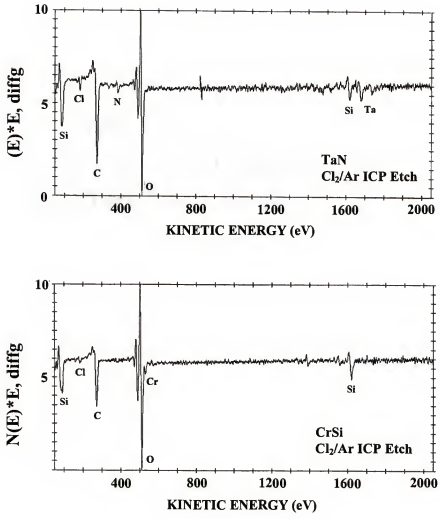

Figure 4-17. AES surface scans of TaN (top) or CrSi (bottom) after ICP etching in $10Cl_2/5Ar$, 2mTorr, -100V dc self-bias, 750W source power discharges.

iodine concentrations. The rate-limiting step appears to be removal of the $FeCl_x$ and FeI_x etch products, based on the low etch rate of the Fe layers. Indeed for very high ICl percentages, there is net deposition on the Fe due to the inability to effectively remove the chloride etch products. Note also that as the ICl percentage in the discharge increases, the chuck self-bias also increases. This indicates that the positive ion density in the plasma is decreasing,[48] as expected since both chlorine and iodine are electronegative gases.

The results for IBr/Ar discharges are shown at the bottom of Figure 4-18. The etch rate behavior for Ni is similar to that with ICl/Ar, but the Fe etches much more rapidly in IBr/Ar discharges, especially at high halogen concentrations. This is due to the higher volatility of the $FeBr_x$ etch products relative to $FeCl_x$,[47] and is not a strong function of bias. This effect leads to a small increase in NiFe and NiFeCo etch rate at IBr percentages beyond ~ 60%.

The effect of ICP source power on the material etch rates is shown for ICl/Ar (top) and IBr/Ar (bottom) in Figure 4-19. For the ICl/Ar, the etch rates for Ni, NiFeCo and NiFe increase monotonically with increasing ion flux, even though the self-bias decreases because of the larger conductivity of the plasma. For Fe there is essentially no etching until source powers >600W, which illustrates the point that balancing the ion and reactive neutral fluxes can lead to a positive etch rate.[46] The behavior of NiFe and NiFeCo in IBr/Ar discharges is basically similar to that with ICl/Ar. The Ni and Fe etch rates go in different direction at high flux, due to the ion energy falling below that needed to efficiently desorb $NiBr_x$ and NiI_x. The low rates may also be attributed to the chemical

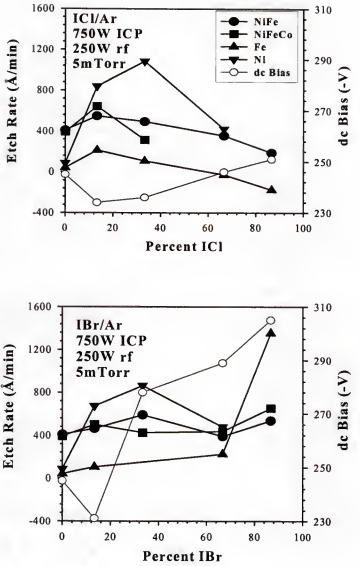

Figure 4-18. Etch rates of Ni, Fe, NiFe and NiFeCo in 750W source power, 250W rf chuck power, 5mTorr discharges of ICl/Ar (top) or IBr/Ar (bottom), as a function of plasma composition.

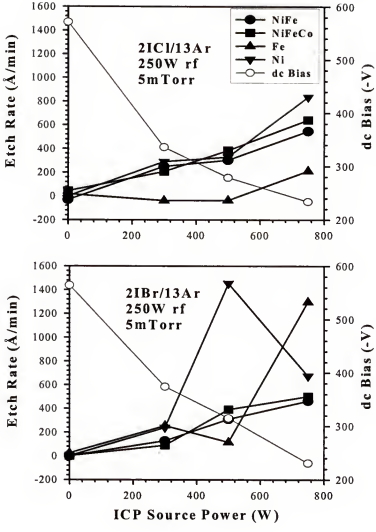

Figure 4-19. Etch rates of Ni, Fe, NiFe and NiFeCo in 250W rf chuck power, 5mTorr discharges of 2ICl/13Ar (top) or 2IBr/13Ar (bottom), as a function of source power

kinetics of the reaction. Under high flux conditions, the reactive species may sputter off the surface prior to reaction.

The dependence of material etch rates on rf chuck power is shown in Figure 4-20 (top) for 2ICl/13Ar and Figure 4-20 (bottom) for 2IBr/13Ar discharges at fixed source power (750W) and pressure (5mTorr). For both chemistries the etch rates (except those for Ni) are basically linearly dependent on chuck power, indicative of a desorption-limited process. For Ni in both chemistries and Fe in IBr/Ar, the rates initially increase as the rf chuck power (and hence dc self-bias is increased), but then decrease beyond particular maxima. This is often observed in high density plasma etching of materials, and is usually ascribed to desorption of the adsorbed chlorine neutrals before they can react with the surface of the metal.[37] The reaction rate is presumably different on the alloys, where this trend is not observed up to our maximum of chuck power.

Figure 4-21 shows the pressure dependence of material etch rates in 2ICl/13Ar discharges (750W source power, 250W rf chuck power). We were not able to produce stable IBr/Ar discharges at pressures above 5mTorr. Even though dc self-bias increases with pressure, the etch rates of all of the materials decrease with increasing pressure. We suspect that the ion/neutral ratio falls below that necessary for effective balance of the product formation and desorption. Once again, the rate-limiting step is removal of the Fe. The etch yields and ion fluxes calculated from the etch rate and dc self-bias on the chuck are shown at the bottom of the Figure.[49] The low etch yields show why high density plasma conditions are needed to produce practical etch rates for the magnetic materials.

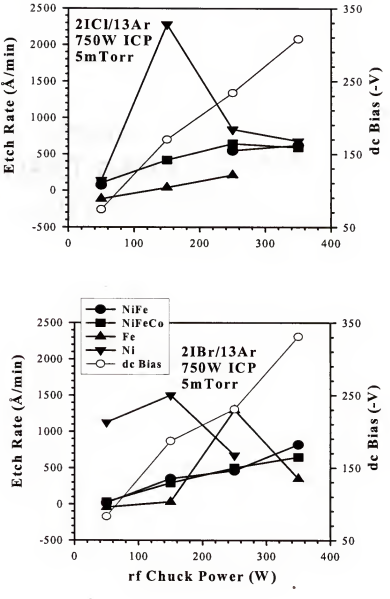

Figure 4-20. Etch rates of Ni, Fe, NiFe and NiFeCo in 750W source power, 5mTorr discharges of 2ICl/13Ar (top) or 2IBr/13Ar (bottom), as a function of rf chuck power.

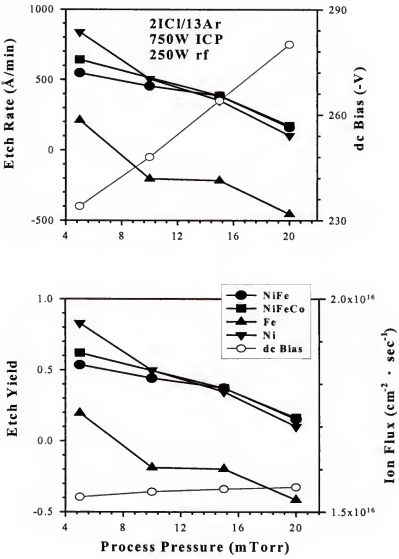

Figure 4-21. Etch rates (top) and etch yields (bottom) of Ni, Fe, NiFe and NiFeCo in 2ICl/13Ar, 750W source power, 250W rf chuck power discharges, as a function of process pressure.

The surfaces of the NiFe and NiFeCo were smooth over a broad range of plasma conditions. Figure 4-22 shows AFM scans from NiFe samples after etching of ~ 2000Å of material in IBr/Ar discharges (750W source power, 250W rf chuck power, 5mTorr) at different gas compositions. The as-grown root-mean-square (RMS) roughness is ~ 0.55nm. At low IBr compositions the surface is significantly rougher (1.8nm RMS), but as the chemical component of the etching increases the surfaces are as good or slightly better than the control value. A similar trend was observed with NiFeCo layers, as shown in Figure 4-23. The main difference is that even for the low IBr concentration the RMS roughness is still as good as the control value. These data show there is a wide process window for maintaining high quality surfaces with the interhalogen plasma chemistries. The AES data showed that the samples retained their initial stoichiometry under these conditions.

The surfaces were also relatively clean after etching. Figure 4-24 shows AES surface scans of NiFe after either ICl/Ar (top) or IBr/Ar etching (center and bottom) at different plasma compositions. We observe adventitious carbon and a native oxide originating from exposure to ambient during transfer from etch chamber to analysis chamber. There is only a slightly amount of residual chlorine detected on the ICl etched material ($\leq$1 at. %), which is consistent with the mechanism involving efficient desorption of the etch products by the attendant ion flux. There was no Br (main Auger transition at 1396eV) detected on any of the samples, while any I signal would be swamped by that due to oxygen (iodine transition at 511eV).

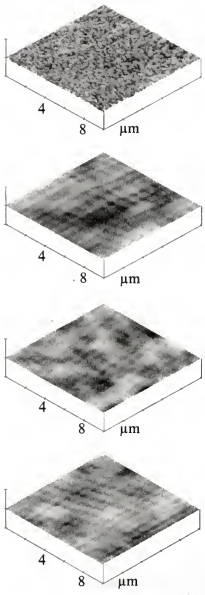

Composition	RMS roughness
2IBr/13Ar	1.789nm
5IBr/10Ar	0.550nm
10IBr/5Ar	0.594nm
13IBr/2Ar	0.328nm

Figure 4-22. AFM scans of NiFe after etching in 750W source power, 250W rf chuck power, 5mTorr discharges, as a function of plasma composition.

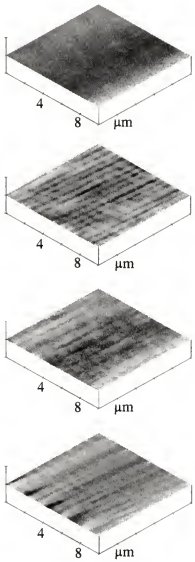

Figure 4-23. AFM scans of NiFeCo after etching in 750W source power, 250W rf chuck power, 5mTorr discharges, as a function of plasma composition.

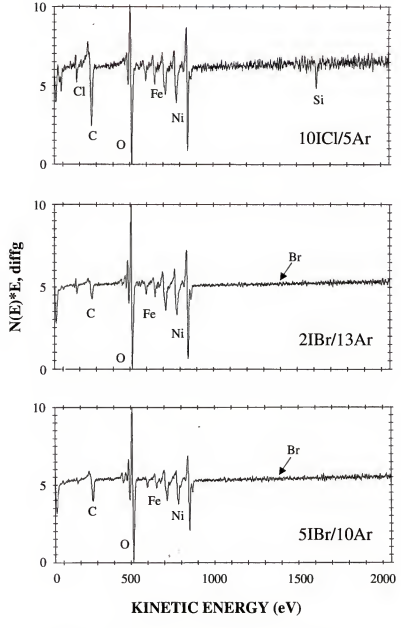

Figure 4-24. AES surface scans of NiFe after etching in either ICl/Ar (top) or IBr/Ar (center and bottom) discharges (750W source power, 250W rf chuck power, 5mTorr), as a function of plasma composition.

Similar data was obtained for etched NiFeCo samples. Once again the surfaces were relatively clean, with residual bromine concentrations below the detection limit of AES.[35,46] We have previously reported that use of in-situ H_2 plasma cleaning is effective in volatilizing halogen residues, producing clean surfaces on the etched field.[35] More work needs to be done to establish the chemical state of the sidewalls of etched features, since this is what will determine the extent of long-term corrosion on patterned magnetic multilayers.

4.4.3. Effect of Inert Gas Additive on Cl_2-based Plasma Chemistries

We compared the effectiveness of He, Ar and Xe additives to ICP Cl_2 plasmas for etching NiFe and NiFeCo, and in terms of the amount of residual chlorine remaining on the etched surfaces. While the same basic trends in etch rate were observed with variation of ICP source power, rf chuck power and pressure, we found less residual chlorine on Cl_2/He exposed NiFe and NiFeCo surfaces.

Figure 4-25 shows the influence of ICP source power on the etch rates of NiFe and NiFeCo in the three different plasma chemistries at fixed Cl_2:noble gas composition (2/13), rf chuck power (250W) and pressure (5mTorr). Note that at zero source power, which corresponds to conventional reactive ion etching, there is net deposition occurring on the samples as discussed earlier. As the source power increases, both the ion flux and the atomic chlorine neutral flux incident on the surface of the magnetic materials will increase, producing higher etch rates. However, a competing effect is the reduction in dc self-bias on the sample chuck as the conductivity of the plasma increases, leading to less

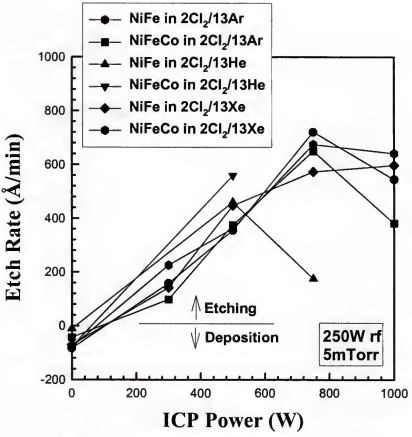

Figure 4-25. Etch rates of NiFe and NiFeCo in ICP Cl_2-based discharges at fixed composition, pressure (5mTorr) and rf chuck power (250W), as a function of source power.

effective ion-assisted desorption of the etch products. Under our conditions, this dc bias decreases from -308V at 0W source power, to -126V at 1000W source power. The net result of the competition between increasing ion flux and decreasing ion energy as the source power is increased is that the etch rates go through a maximum for each plasma chemistry. As expected, the maximum will occur at lower source powers for Cl_2/He, due to the lighter mass of the helium relative to the other two inert gases. At the highest source power investigated (1000W), Xe addition produces slightly faster etch rates than Ar addition.

The influence of rf chuck power on NiFe and NiFeCo etch rates in the three plasma chemistries at fixed source power (750W) and pressure (5mTorr) is shown in Figure 4-26. As chuck power increases, the dc self-bias also increases (from approximately -35V at 50W to -217V at 350W). The etch rates of both materials show a monotonic increase as chuck power increases up to ~250W, since the average ion energy is also increasing. The reduction in etch rates beyond 250W is most likely due to ion-assisted desorption of the chlorine neutrals before they can react with the surface of the magnetic materials. This is the same trend commonly observed in high density plasma etching of many different types of materials, but is usually not seen in conventional reactive ion etching due to the much lower ion fluxes in the latter technique. The etching becomes reactant-limited under these conditions, i.e. an increase in flow rate or pressure produces faster rates, consistent with the mechanism discussed above.

The role of process pressure is shown in Figure 4-27. For clarity we have shown only the data for Cl_2/Xe, at fixed source power (750W) and rf chuck power (250W). The rates for both NiFe and NiFeCo decrease with increasing pressure. The self-bias increases

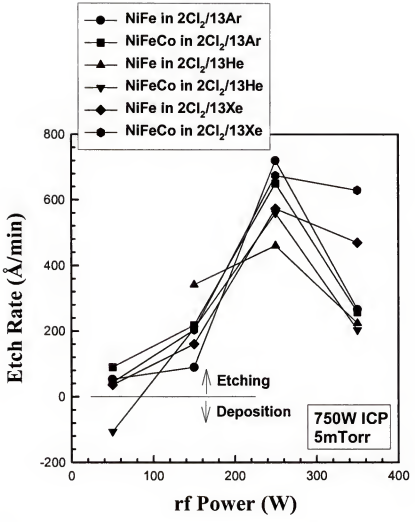

Figure 4-26. Etch rates of NiFe and NiFeCo in ICP Cl_2-based discharges at fixed composition, pressure (5mTorr) and source power (750W), as a function of rf chuck power.

slightly over the pressure range due to a reduced ion density because of reattachment of electrons with ions, and we assume the decrease in etch rates results from the decreased ion and reactive neutral flux since this is the available mechanism to produce slower rates. We have also included data for single Ni and Fe layers in Figure 4-27, to show that Fe is the most difficult material to remove in Cl_2-based plasmas, and limits the etch rate of NiFe (and NiFeCo).

A key point of interest is whether the surface of the etched material remains smooth, both from the view point of subsequent processing and the fact that this is at least an indication of whether each component element is being removed at the same rate. Figure 4-28 shows AFM images taken in tapping mode of NiFe layers after etching ~2000Å in Cl_2/He, Cl_2/Ar or Cl_2/Xe in 750W source power, 250W rf, 5mTorr discharges. The as-grown sample is relatively rough (root-mean-square, RMS, of 7nm) because the film is so thick. The etched samples have fairly similar morphologies, and indeed in the case of Cl_2/He, the RMS value is better than that of the control sample. This can occur in dry etching methods, particularly when there is a high physical component to the etching, because of the angular dependence of ion milling rates leading to more rapid removal of sharp features.

Similar data is shown in Figure 4-29 for NiFeCo. In this case the etched surfaces are rougher than those of the control, with the RMS values becoming worse with the heavier mass of the inert gas species. Surface smoothness is very important from a micromagnetic point of view, as rough surfaces generally show hysteresis loop broadening, as also would a stoichiometric shift causing increased magnetostriction and/or magnetocrystalline anisotropy to become effective.

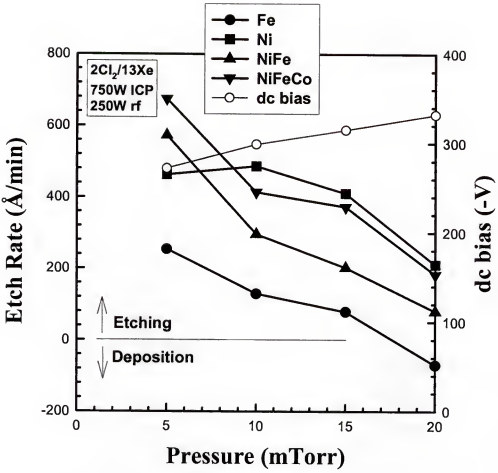

Figure 4-27. Etch rates of NiFe, NiFeCo, Ni and Fe in ICP $2Cl_2$/13Xe discharges (750W source power, 250W rf chuck power), as a function of process pressure.

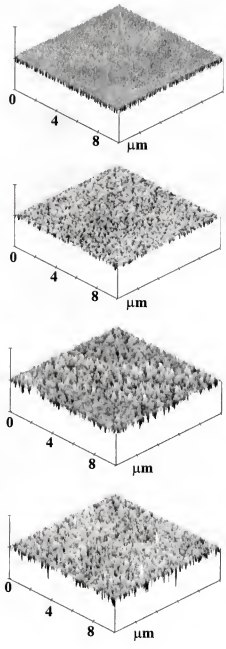

Figure 4-28. AFM scans of NiFe surfaces before and after etching in Cl_2/He, Cl_2/Ar or Cl_2/Xe ICP discharges fixed source power (750W), rf chuck power (250W) and pressure (5mTorr). Z-scale is magnified for the etched samples.

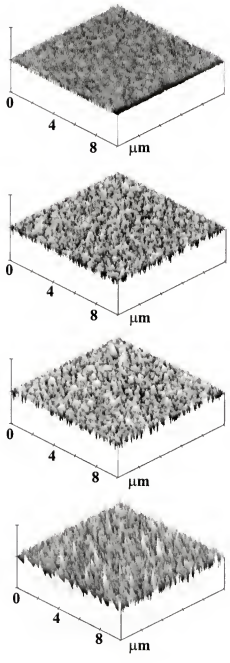

Figure 4-29. AFM scans of NiFeCo surfaces before and after etching in Cl_2/He, Cl_2/Ar or Cl_2/Xe ICP discharges fixed source power (750W), rf chuck power (250W) and pressure (5mTorr). Z-scale is magnified for the etched samples.

Auger Electron Spectroscopy (AES) was employed to examine the near-surface stoichiometry of the etched samples. Figure 4-30 shows surface scans from the NiFe samples etched in the three different plasma chemistries under the same conditions as the AFM samples of Figure 4-28. There is less chlorine residue remaining on the Cl_2/He sample, in good correlation with the smoother surface under these conditions. The depth profiles showed that the Ni and Fe profiles were constant beyond the top ~50Å of the surface. The same results were obtained for the NiFeCo samples. It appears that Cl_2/He provides the optimum ratio of ion flux to chlorine neutral density at the particular set of plasma parameters employed here.

Figure 4-31 shows AES surface scans from the NiFeCo samples, with the least chlorine residue measured on the Cl_2/He etched material. For our set of conditions, this plasma chemistry produces the best balance of $NiCl_x$, $FeCl_x$ and $CoCl_x$ etch products formation combined with efficient ion-assisted desorption.

As an example of features etched into NiFe using this process, Figure 4-32 shows SEM micrographs of SiO_2-masked structures. The samples were rinsed in water immediately after removal from the plasma reactor to remove residual chlorine , in order to prevent subsequent corrosion. The feature sidewalls are relatively smooth and there is no apparent redeposition.

4.4.4. Long-Term Stability after Etching and Post-Etch Treatments

In Cl_2/Ar high density plasmas, the high ion flux is able to provide efficient ion-assisted desorption of metal-chloride etch products, through a balance of etch product formation and removal. However one concern with this process is the effect of residual

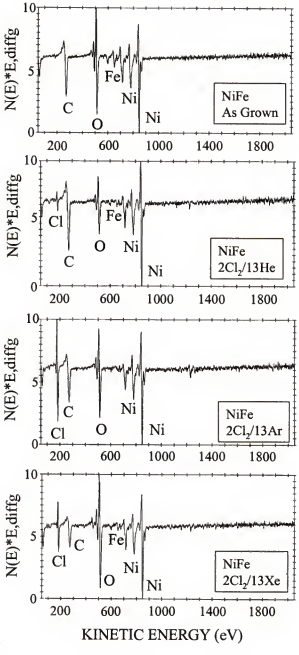

Figure 4-30. AES surface scans of NiFe surfaces before (first), or after etching in $2Cl_2$/13He (second), $2Cl_2$/13Ar (third) or $2Cl_2$/13Xe (fourth) ICP discharges at fixed source power (750W), rf chuck power (250W) and pressure (5mTorr).

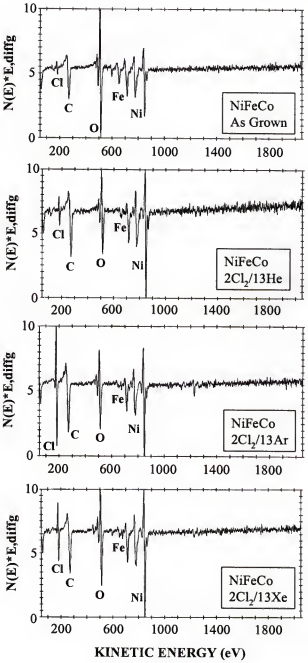

Figure 4-31. AES surface scans of NiFeCo before (first), and after etching in ICP discharges (750W source power, 250W rf chuck power, 5mTorr) of $2Cl_2$/13He (second), $2Cl_2$/13Ar (third) and $2Cl_2$/13Xe (fourth).

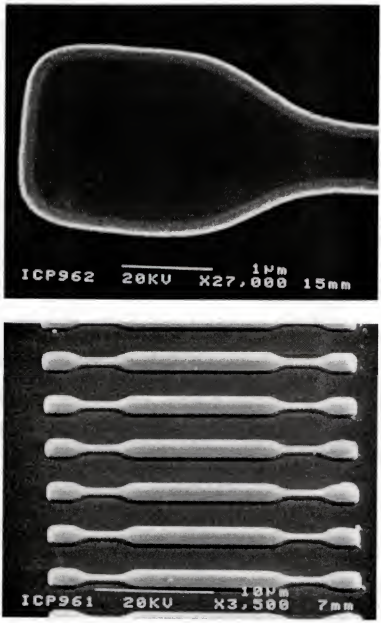

Figure 4-32. SEM micrographs of features etched into NiFe using $2Cl_2/13Ar$, 5mTorr, 750W source power, 250W rf chuck power ICP discharges. The SiO_2 masks are still in place.

chlorine or chlorinated etch residues remaining on the sidewalls of etched features. In this paper we report on the effectiveness of several different in-situ or ex-situ cleaning processes after Cl_2/Ar high density plasma etching of GMR elements.

Most of the experiments were performed with the MRAM structure shown in Figure 4-33. The SiO_2 and SiN_X layers were grown on Si substrates by chemical vapor deposition, followed by Ar^+ ion-assisted sputtering of the magnetic multilayers. The structure was completed with anti-oxidation and contact layers (Ta, TaN, CrSi) and a 3000Å thick SiO_2 mask patterned by SF_6/Ar RIE was employed as the etch mask for ICP etching. In some cases we also deposited single, 500Å thick, layers of Ni, $Ni_{0.8}Fe_{0.2}$ or $Ni_{0.8}Fe_{0.13}Co_{0.07}$ on Ta buffers on Si substrates to examine their magnetic properties after dry etching.

It has previously been found that the coercivity of MRAM elements can be severely increased (by up to a factor of eight) when high energy (1000eV) Ar^+ ion milling is used for pattern transfer, relative to lower energy (300eV) milling.[50] Under our ICP conditions, the average incident ion energy is ~200eV.[37] To examine the effect of this ion bombardment on magnetic properties, the single layer Ni, NiFe and NiFeCo samples were exposed to the ICP Ar discharge. The sputter rate of all three films was ~8Å·sec^{-1} under our conditions. Figure 4-34 shows the saturation magnetization to be independent of remaining Ni, NiFe or NiFeCo thickness, which indicates the plasma exposure is not creating significant "magnetically-dead" regions ahead of the etch-front. We note that damage in this direction vertical to the incoming ion is expected to be much worse than damage to the sidewalls of etched features, due to the low process pressure (2mTorr) and

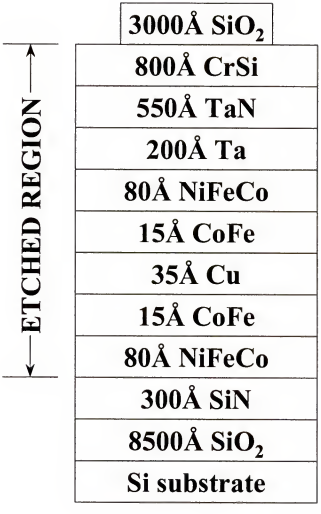

Figure 4-33. Layer structure of MRAM element. The top SiO_2 layer is the mask for ICP etching of the underlying layers. Etching terminates on the 300Å thick SiN_X layer.

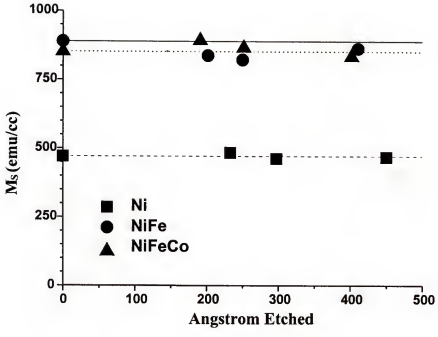

Figure 4-34. Saturation magnetization versus thickness removed by etching in 500Å thick films of Ni, NiFe and NiFeCo.

consequent minimization of ion scattering that might cause divergence from the expected vertical angle of incidence. Moreover, in a real etch process there would be less damage due to the presence of some chemical enhancement and consequent higher etch rate,[47] reducing the possibility of damage accumulation.

Turning to the Cl_2/Ar etched MRAM stacks, we have previously found that severe corrosion occurs on the edges of the elements if no specific steps are taken to avoid this,[15] as shown in the SEM micrographs of Figure 4-35. In this case the samples were patterned with the Cl_2/Ar process, and simply stored in air. The SEM micrographs were taken approximately two weeks later, and show the classic signs of metal corrosion.

To counteract this problem, four different post-etch treatments were examined. The first was simply rinsing the samples in de-ionized water immediately upon opening the chamber (which is contained within a N_2 dry box). The samples were then thoroughly dried with filtered N_2. In the other three methods, various in-situ plasma cleaning procedures were examined. After the Cl_2/Ar etching was complete, the chamber was evacuated for 15mins, and then a 30mTorr discharge of either H_2, O_2 or SF_6 (500W source power, 5W chuck power) was used to clean the residual chlorine for 10mins prior to removed or the samples from the reactor. In these cases, no H_2O rinsing was performed. It should be pointed out that all of these cleaning procedures have been employed previously for removing etch residues after Cl_2-based plasma etching of Al interconnects in Si microelectronics.[51]

Figure 4-36 shows some typical SQUID data for MRAM samples before and after Cl_2/Ar etching and subsequent cleaning. We assume the hysteresis in the control sample

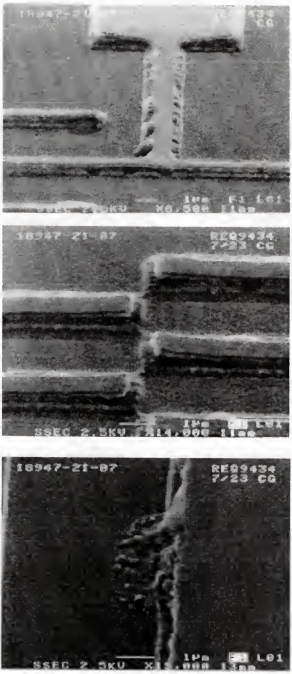

Figure 4-35. SEM micrographs of Cl_2/Ar etched MRAM elements taken about two weeks after etching. For these samples, no post-etch cleaning of chlorine residues was performed.

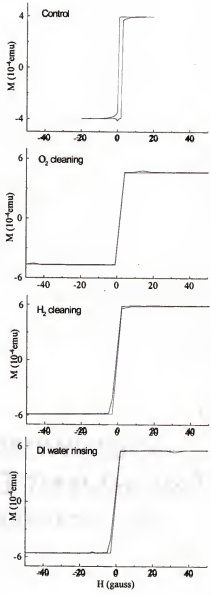

Figure 4-36. Hysteresis loops for MRAM structure before and after ICP Cl_2/Ar etching, and subsequent cleaning for 10mins either by H_2O rinsing or exposure to H_2 or O_2 plasmas prior to removal from the etch reactor.

is related to some inhomogeneity in materials properties, relative to the smaller volume sampled in the patterned structures. The data for the SF_6 cleaned sample was similar to that for H_2 cleaning. The data was normalized to the remaining volume of magnetic material after patterning, and the results are shown in Figure 4-37. Within experimental error, there is no change in the magnetization per unit volume for any of the samples except that treated in O_2. A possible interpretation of this is that the feature sidewalls become more oxidized than with the other treatments, leading to a degradation of the magnetic properties. The results of Figure 4-37 are clear evidence that a magnetic multilayer structure can be patterned by dry etching under optimized conditions (i.e. post-etch H_2O rinse, or H_2 or SF_6 in-situ plasma cleaning) without any fall-off in the magnetic performance of the structure.

We believe the fall-off in magnetization of the O_2 plasma exposed sample is not a result of residual chlorine and subsequent corrosion for two reasons. Firstly, Figure 4-38 shows AES surface scans of single layer NiFe samples exposed to the Cl_2/Ar discharge, and then cleaned for 5mins using the different treatments material above. There are significant amount of residual chlorine on the H_2 and SF_6 treated samples, but with either water rinsing or O_2 plasma exposure, the Cl_2 signal is at the detection limit. These results show that O_2 is more effective per unit time in removing chlorine residues than either H_2 or SF_6. The second reason is the excellent long-term stability of all of the cleaned samples, showing that there is no corrosion. After 10 min cleans (as used in the final, optimized process), we detected only the lattice elements on each sample and no Cl-related residues were found.

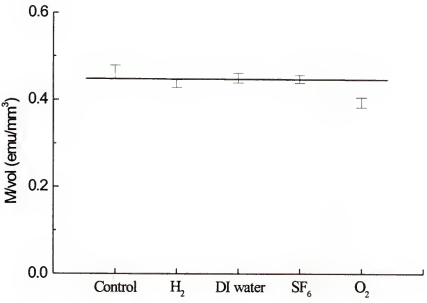

Figure 4-37. Magnetization per unit volume for MRAM structure before and after ICP Cl_2/Ar etching, and subsequent cleaning for 10mins either by H_2O rinsing or exposure to H_2, SF_6 or O_2 plasmas prior to removal from the etch reactor.

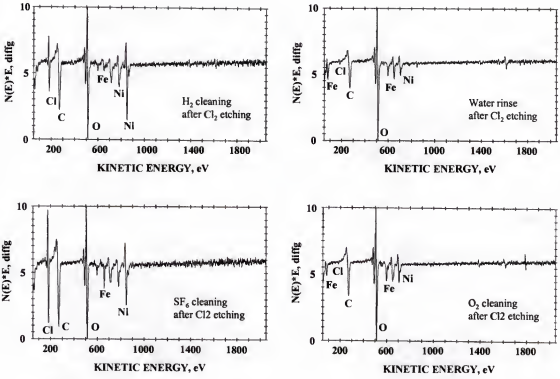

Figure 4-38. AES surface scans from NiFe samples exposed to ICP Cl_2/Ar plasmas and subsequently cleaned for 5mins either by H_2O rinsing or exposure to H_2, SF_6 or O_2 plasmas prior to removal from the etch reactor.

Figure 4-39 shows the magnetization of each of the samples over an extended period. In each case the samples were simply stored in air between the measurements and no special precautions were taken to prevent corrosion. Each of the cleaning procedures produces samples with extremely stable magnetic characteristics. This is also reflected in their appearance. The control sample was similarly stable with time. If we did not use any of the cleaning procedures after dry etching, corrosion quickly (<7 days) destroyed the samples.[46] Figure 4-40 shows SEM micrographs of patterned MRAM elements 6 months after Cl_2/Ar etching and post-etch cleaning. There is no indication of corrosion on any of the samples.

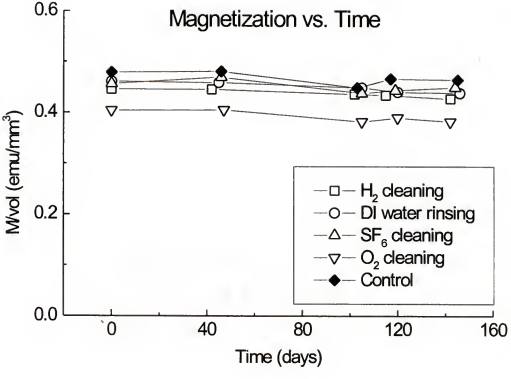

Figure 4-39. Magnetization of MRAM structures, either unetched or etched in ICP Cl/Ar plasmas and subsequently cleaned in H_2O or H_2, SF_6 or O_2 plasmas, as a function of storage time in room ambient.

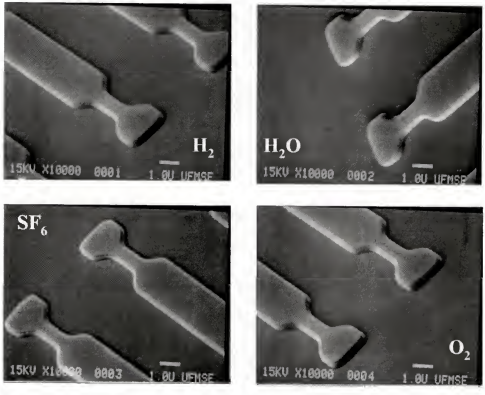

Figure 4-40. SEM micrographs of MRAM elements after etching in ICP Cl_2/Ar plasmas and subsequent cleaning in H_2, SF_6 or O_2 discharges or by H_2O rinsing. The micrographs were taken 6 months after these processes, with the samples having been stored in room ambient.

CHAPTER 5
INDUCTIVELY COUPLED PLASMA ETCHING OF CoFeB, CoZr, CoSm, AND FeMn THIN FILMS

5.1. Introduction

Magnetic multilayers displaying the Giant Magnetoresistance (GMR) effect form the basis of high density data storage systems.[52] Currently, bit storage densities of 11.6GBit·in^{-2} have been demonstrated using GMR heads.[26] At these densities, a read track width on the disk of ~0.7μm, with a sensing layer thickness of 400Å are necessary. In order to increase storage density, reduction of the conducting layer spacer thickness and decrease of the sensing layer coercivity (Hc) are necessary, in addition to reducing the track width. Permalloy ($Ni_{0.8}Fe_{0.2}$) is commonly used as the soft ferromagnetic sensing layer in spin-valve multilayers due to its low coercivity (3Oe). However, amorphous magnetic materials can achieve even lower coercivities due to the absence of grain boundaries, which are a main source of domain-wall pinning. An Hc value of 0.72 has been reported for CoFeB films.[53] Another potential advantage of amorphous ferromagnetic alloys in GMR multilayers is their high electron scattering probability. Amorphous CoFeB may have a resistivity as high as 40μΩ·cm.[54] At the same GMR ratio, higher resistivity material produces a higher resistance change and consequently a higher output signal.

Pattern transfer in magnetic multilayer structures is a critical step in achieving high storage densities. Most etching of magnetic materials is performed using ion milling,

but we have recently found that Cl_2/Ar high density plasmas are capable of overcoming the inherent low volatility of the metal-chloride etch products through efficient ion-assisted desorption.[35,47] All of the work to date has focused on NiFe and NiFeCo, but for the reason outlined above there is interest in extending this to other materials, such as exchange pinning layers (FeMn) and the Co-based sensing layers. In this chapter we report on a comparison of Cl_2/He, Cl_2/Ar and Cl_2/Xe Inductively Coupled Plasma (ICP) dry etching of CoFeB, CoSm, CoZr and FeMn thin films. The atomic weight of the inert gas additive is found to have a strong influence on the etch rate and surface morphology of these materials.

We also report on an investigation of ICP etching of thin film FeMn, CoFeB, CoZr and CoSm in ICl and IBr plasma chemistries. These gases readily dissociate in high density plasma sources and might produce higher rates than Cl_2-based etching. For example, CoI_2 has a much lower boiling point than $CoCl_2$, suggesting that it would be advantageous to use I_2-containing gases because the iodide etch products would be more volatile.

5.2. Materials and Experimental Procedure

Layers of $(Co_{0.9}Fe_{0.1})_{0.8}B_{0.2}$, $Co_{0.93}Zr_{0.07}$, $Co_{0.9}Sm_{0.1}$ and $Fe_{0.5}Mn_{0.5}$ ~5,000Å thick were deposited on Si wafers by dc magnetron sputtering at a rate of ~0.8Å·sec^{-1} using 2mTorr Ar pressure and pressed powder targets.[55] For etch rate experiments, the samples were masked with Apiezon wax. The etching was performed in a Plasma Therm 790 ICP system. The samples were thermally bonded to a He backside cooled, rf powered (50-350, 13.56MHz) chuck. A 3-turn, 2MHz ICP source operating at 0-1000W generated the

discharges, at process pressures of 5-20mTorr. Electronic grade Cl_2, He, Ar or Xe were injected into the source through mass flow controllers at a total gas load of 15 standard cubic centimeters per minute (sccm). Etch depths obtained from stylus profilometry measurements, and surface roughness was evaluated by tapping mode Atomic Force Microscopy (AFM). The magnetic properties of the CoSm films were measured before and after etching using a SQUID magnetometer (Quantum Design MPMS-55).

5.3. Cl_2-based Plasma Chemistries

Figure 5-1 shows the effect of plasma composition on material etch rates in Cl_2/He discharges (750W source power, 250W chuck power, 5mTorr pressure). The etch rates initially increase as Cl_2 is added, since this provides a chemical component to the etch mechanism. However, beyond a composition of $2Cl_2/13He$ the rates decrease and in some cases there is actually net deposition rather than etching. This is consistent with the proposed mechanism for etching of magnetic materials in Cl_2, namely that the physical and chemical aspects must be balanced. If the ion/neutral ratio becomes too high then the etch mechanism is basically just sputtering, while if this ratio becomes too low, a chlorinated selvedge layer will build-up on the surface and produce net deposition as is the case with conventional reactive ion etching. Note that the chuck self-bias increases as Cl_2 is added, since the electronegative chlorine will reduce the positive ion density in the discharge. However, this increase will produce an increase in average ion bombardment energy, and does not overcome the increase in chlorine neutrals which occurs at high

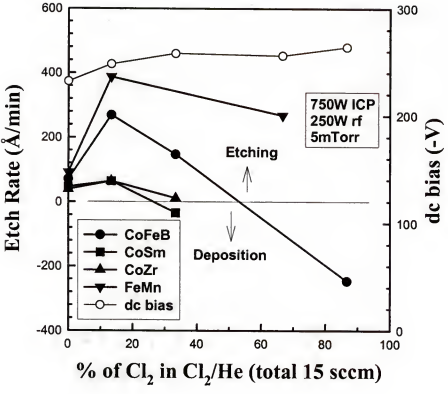

Figure 5-1. Etch rates of CoFeB, CoSm, CoZr and FeMn in ICP Cl_2/He discharges (750W source power, 250W rf chuck power, 5mTorr) as a function of plasma composition.

Cl_2/He ratios. We have previously reported in Electron Cyclotron Resonance (ECR) tools, that the maxima in etch rates occur at an ion-to-neutral flux ratio of ~0.02.[35]

Similar data for the Cl_2/Ar chemistry are shown in Figure 5-2. The same basic trends are observed, with slightly higher sputter rates obtained with Ar relative to He. Note that the etch rate for CoFeB always remains positive over the large of plasma compositions, probably as a result of the more efficient sputter-desorption of chloride etch products by the heavier ions.

Little advantage was gained by replacing Ar with Xe, as shown in Figure 5-3. The peak etch rates are slightly higher, but the same basic behavior was obtained as with the other two inert gas additives. Since Xe is substantially more expensive than the other gases, there does not seem to be compelling reason for its use in dry etching of these magnetic materials.

For examining the effect of the other plasma parameters on etch rate, we settled on a fixed discharge composition of 2 sccm of Cl_2 and 13 sccm of the inert gas. Figure 5-4 shows the influence of ICP source power on material etch rates for Cl_2/He discharges at fixed rf chuck power (250W) and pressure (5mTorr). At low source powers, corresponding to reactive ion etching (RIE)-like conditions, the process is ineffective. However, as the ion density in the discharge increases as source power is increased, the ion-assisted desorption of the metal chlorides becomes effective. Removal of Zr seems to limit the CoZr etch rates. Note that as the ion density increases, dc self bias decreases due to the increased conductivity of the plasma.

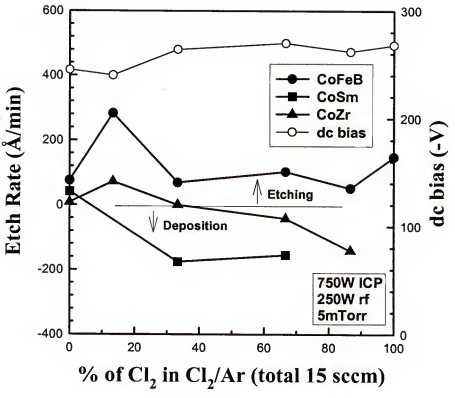

Figure 5-2. Etch rates of CoFeB, CoSm and CoZr in ICP Cl_2/Ar discharges (750W source power, 250W rf chuck power, 5mTorr) as a function of plasma composition.

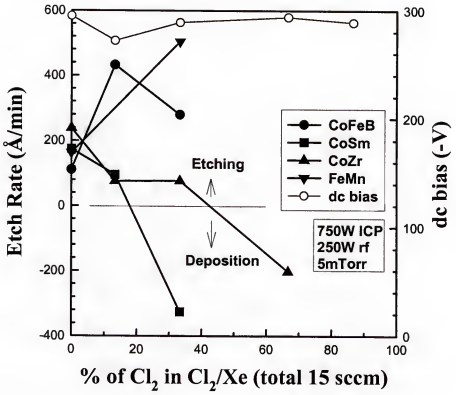

Figure 5-3. Etch rates of CoFeB, CoSm, CoZr and FeMn in ICP Cl_2/Xe discharges (750W source power, 250W rf chuck power, 5mTorr) as a function of plasma composition.

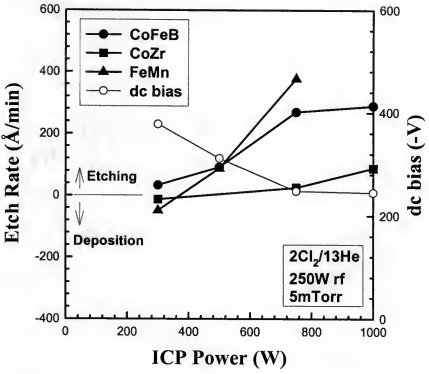

Figure 5-4. Etch rates of CoFeB, CoSm, CoZr and FeMn in ICP $2Cl_2$/13He discharges (250W rf chuck power, 5mTorr) as a function of source power.

The same basic trends were obtained with Cl_2/Ar as a function of source power (Figure 5-5). In this chemistry we observed net deposition on CoSm for all source powers, which suggests the balance of ion flux and chlorine neutral flux is never achieved for this material. The CoFeB etch rate still has not saturated at 1000W source power in Cl_2/Ar, providing a higher maximum etch rate than in Cl_2/He.

The comparable data for the Cl_2/Xe chemistry is shown in Figure 5-6. The trends are again essentially the same as for the other two mixtures, with a transition from deposition to etching as the source power is increased. This clearly shows why high ion density conditions are needed to successfully etch magnetic materials near room temperature. The high ion flux provides the energy needed to desorb the etch products. Under RIE conditions, we would need to artificially heat the sample to desorb the metal chlorides, but this is unacceptable in thin multilayer structures because of their limited thermal stability.

Figure 5-7 shows the effect of rf chuck power, which controls ion energy, on the magnetic material etch rates in $2Cl_2$/13He discharges at fixed source power (750W) and pressure (5mTorr). At low rf powers, the incident ion energy is below the threshold for etch product desorption in the case of CoFeB and CoZr. As the ion energy increases, this desorption becomes more efficient and etch rate increases. However if the ion energy is too high we see a typical result for high density etching, namely that the rates decrease again due to sputter desorption of the chlorine neutrals before they can react with the surface.

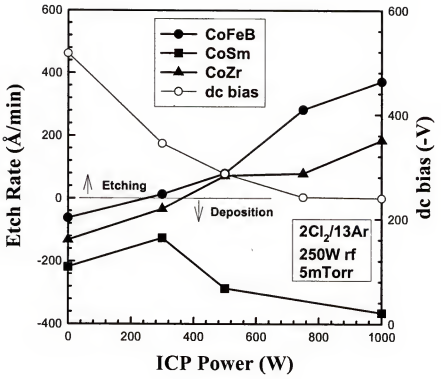

Figure 5-5. Etch rates of CoFeB, CoSm and CoZr in ICP $2Cl_2/13Ar$ discharges (250W rf chuck power, 5mTorr) as a function of source power.

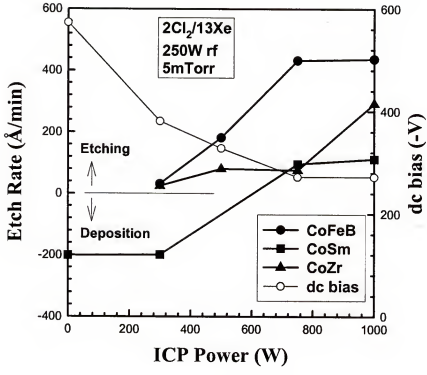

Figure 5-6. Etch rates of CoFeB, CoSm and CoZr in ICP $2Cl_2$/13Xe discharges (250W rf chuck power, 5mTorr) as a function of source power.

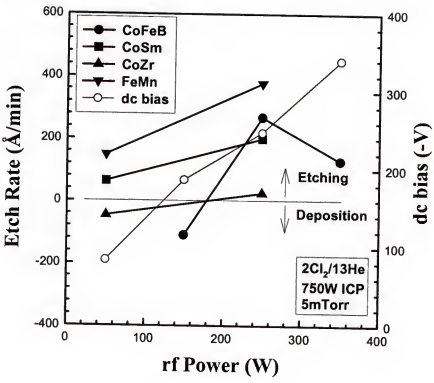

Figure 5-7. Etch rates of CoFeB, CoSm, CoZr and FeMn in ICP $2Cl_2/13He$ discharges (750W source power, 5mTorr) as a function of rf chuck power.

These two key points, i.e., that there is a threshold ion energy for the onset of etching and that the etch rates can decrease if the ion energies are beyond a particular optimum value for each material, are again illustrated in the data for Cl_2/Ar (Figure 5-8). However for this chemistry we once again do not achieve etching of the CoSm, regardless of rf chuck power. The etch rate saturation points are pushed to higher chuck powers for the Cl_2/Xe discharges, as shown in Figure 5-9. One would expect ion energy to be critical in a desorption-limited etch regime as is the case with magnetic materials in Cl_2-based plasmas. The average energy of incident ions is the sum of the voltage through which they are accelerated (i.e. the dc self-bias) plus the plasma potential. The latter is only 20-30eV for ICP discharges. Thus the threshold ion energies for the onset of etching in Cl_2/Xe are ~125eV for CoFeB, ~250eV for CoZr and ~275eV for CoSm.

The value of low pressure conditions for etching the magnetic materials is evident from the data of Figure 5-10. Even though the bias increases slightly, the higher neutral density and reduced ion density lead to a dramatic fall-off in etch rates at higher pressure. This was also observed previously with NiFe and NiFeCo etching.[46] From data on single element layers of the components of the magnetic materials, the rates increase in the order B>Sm>Zr>Fe in Cl_2-based plasmas.

From the viewpoint of subsequent processing and the fact that this is a good indication of whether each component element is being removed at the same rate, the etched surface morphology is important. Figure 5-11 shows AFM images of CoFeB after etching in Cl_2/He, Cl_2/Ar and Cl_2/Xe discharges (750W source power, 250W rf chuck

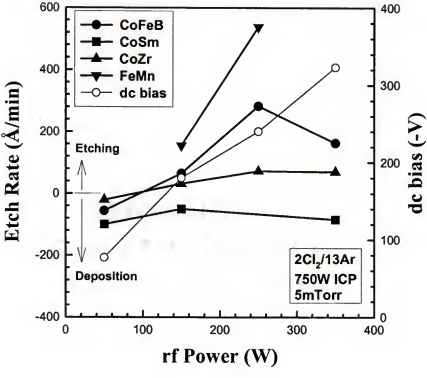

Figure 5-8. Etch rates of CoFeB, CoSm, CoZr and FeMn in ICP $2Cl_2/13Ar$ discharges (750W source power, 5mTorr) as a function of rf chuck power.

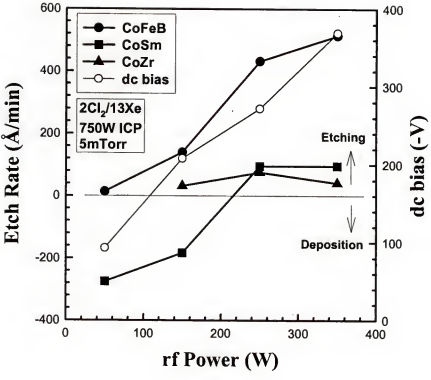

Figure 5-9. Etch rates of CoFeB, CoSm, and CoZr in ICP $2Cl_2/13Xe$ discharges (750W source power, 5mTorr) as a function of rf chuck power.

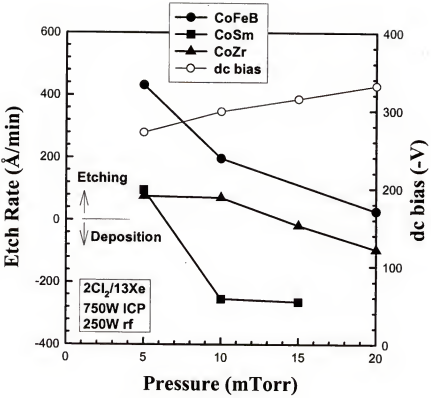

Figure 5-10. Etch rates of CoFeB, CoSm and CoZr in ICP $2Cl_2/13Xe$ discharges (750W source power, 250W rf chuck power) as a function of pressure.

power, 5mTorr). The smoothest surfaces were obtained with Ar and Xe addition, suggesting that these provide the necessary ion-assisted desorption of etch products to maintain the initial surface quality. Similar trends were observed for FeMn, as shown in Figure 5-12.

5.4. Inter-Halogen Plasma Chemistries

Figure 5-13 shows the effect of ICl (top) or IBr (bottom) percentage on material etch rates in ICl/Ar or IBr/Ar discharges at fixed source power (750W), rf chuck power (250W) and pressure (5mTorr). The dc bias increases in both chemistries as the interhalogen percentage increases, indicating that the positive ion density is decreasing. This is expected due to the electronegative character of both ICl and IBr. For FeMn, there is net deposition for ICl percentages up to ~ 66%, while with IBr the etch rates for FeMn obtained with both chemistries (~ 1000Å·min^{-1}) are significantly higher than those obtained with Cl_2/Ar under the same conditions (~ 200Å·min^{-1}), suggesting the metal bromide and iodide etch products are more volatile than their chloride counterparts.[56] The other three materials CoZr, CoFeB and CoSm all show maxima in their etch rates in ICl/Ar, which reflects the balance required between having sufficient reactive neutrals to provide a chemical enhancement in the etch mechanism, and having too many of these neutrals, which blocks the surface to ion bombardment.[35] In each case, the maximum etch rates are higher than those obtained with Cl_2/Ar (~ 300Å·min^{-1} for CoFeB, ~ 80Å·min^{-1} for CoZr and ~ 30Å·min^{-1} for CoSm).[56] The same result is found for the IBr/Ar chemistry, which is particularly effective for etching CoSm.

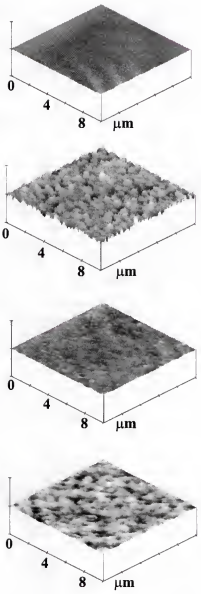

Figure 5-11. AFM scans of CoFeB surfaces before (top) and after etching in Cl_2/He, Cl_2/Ar or Cl_2/Xe 750W source power, 250W rf chuck power, 5mTorr discharges.

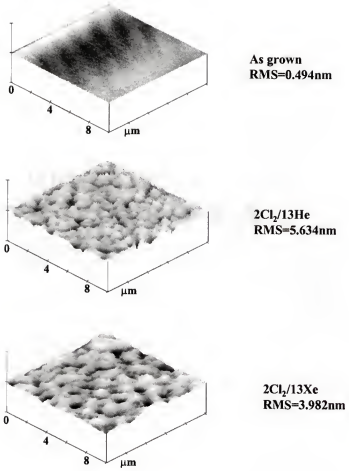

Figure 5-12. AFM scans of FeMn surfaces before (top) and after etching in Cl_2/He or Cl_2/Xe 750W source power, 250W rf chuck power, 5mTorr discharges.

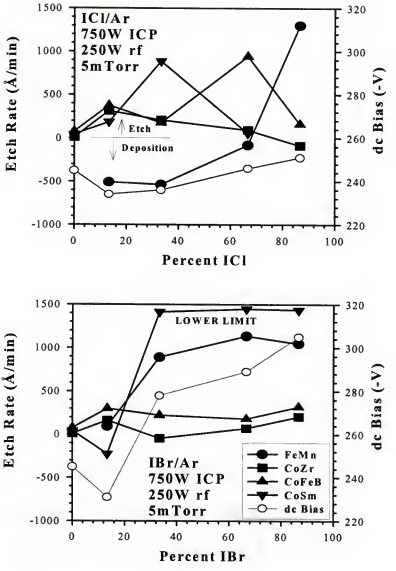

Figure 5-13. Etch rates of CoFeB, CoSm, CoZr and FeMn in ICl/Ar (top) or IBr/Ar (bottom) ICP discharges as a function of interhalogen composition.

Figure 5-14 shows the influence of ICP source power on material etch rates at fixed plasma composition (2 sccm of the interhalogens, 13 sccm of Ar), rf chuck power (250W) and pressure (5mTorr). The dc self-bias decreases as the conductivity (ion density) of the plasma increases. This leads to two competing trends- a certain amount of ion energy is required in most cases to efficiently desorb the metal etch products so that etch rate will fall-off at higher source power if this is the most important factor, but higher ion flux will produce higher etch rates provided ion energy is above the threshold for product desorption. These two phenomena produce the behavior in Figure 5-14, where the rates either increase or decrease with source power. Note that by correct choice of conditions, it would be possible to selectively etch the Co-based materials and stop at an FeMn layer using ICl/Ar, or going in the reverse direction one could selectively etch FeMn and stop at a Co-containing layer using IBr/Ar.

Figure 5-15 shows the effect on etch rates of rf chuck power, which controls the average energy of incident positive ions. The self-bias represents the voltage through which ions are accelerated as they cross the plasma sheath, and the ion energy therefore consists of the sum of this voltage and the plasma potential (which is in the range 20-30eV for ICP discharges).[48] The ion energy can also influence the etch rate in two ways- firstly, the sputtering efficiency of etch products should increase as ion energy is increased, leading to higher rates. Secondly, however, if this energy becomes too high it can lead to desorption of the reactive neutrals before they can react with the surface of the magnetic material. Thus, in Figure 5-15 it is seen that the etch rates can actually decrease at high rf chuck power. In the case of ICl/Ar etching of FeMn, there is a clear threshold for the onset of etching at ~ 300W rf chuck power.

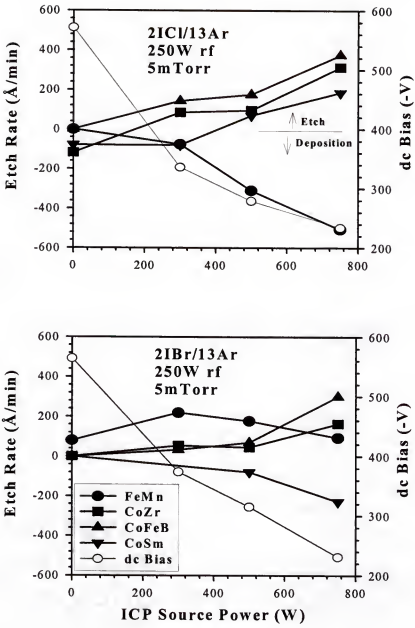

Figure 5-14. Etch rates of CoFeB, CoSm, CoZr and FeMn in 2ICl/13Ar (top) or 2IBr/13Ar (bottom) ICP discharges as a function of source power.

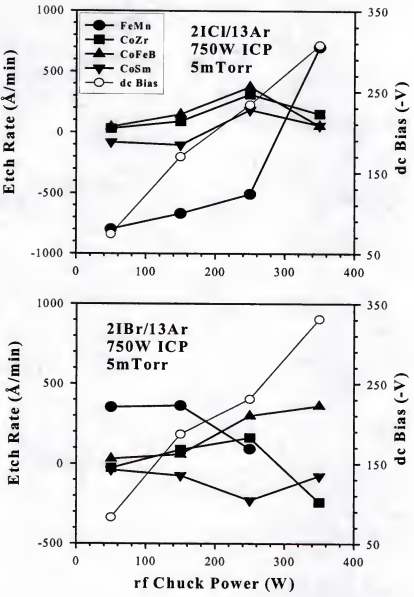

Figure 5-15. Etch rates of CoFeB, CoSm, CoZr and FeMn in 2ICl/13Ar (top) or 2IBr/13Ar (bottom) ICP discharges as a function of rf chuck power.

The etch rates were found to decrease with increasing process pressure, as shown in Figure 5-16. As pressure increases there will be more recombination in the discharge and a higher number of adsorbed neutrals blocking the surface from ion bombardment. The etch yields were calculated from a simple model, and are shown in the lower part of Figure 5-16. Under these conditions they are < 0.4 for all the materials, showing that the etching still requires a strong physically-assisted component.

A primary concern with new etch processes for magnetic materials is whether there is a change in the properties of the material due to ion bombardment damage. For example, ion milling at 1000eV Ar^+ energy was found to damage submicron GMR cells for non-volatile memories; the coercivity of arrays of pseudo spin valve bits was found to increase by a factor of 8 for ion milling at 1000eV compared to 300eV.[50] In our chemically-assisted process we would expect less damage than in purely physical etching. To confirm this, magnetic hysteresis loops were obtained for the CoSm films with the field applied both parallel and perpendicular to the film plane. Typical coercive fields for our film were in the range H_c = 4-9kO_e for both parallel and perpendicular directions.

Figure 5-17 shows the effect of ICP source power on the magnetic properties of the CoSm exposed to pure Ar discharges for 1min. This would simulate a worst-case scenario of ion bombardment with no chemical component to the etching. Within experimental error we see no change in the magnetic properties of our films. Similarly, it is seen in Figure 5-18 that rf chuck power does not produce any degradation of magnetic properties. We caution that we are measuring only the blanket films, and not patterned structures which would be expected to be more sensitive to changes due to plasma etching.

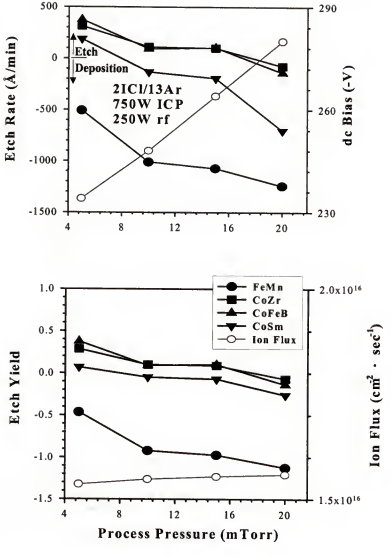

Figure 5-16. Etch rates (top) and etch yields (bottom) of CoFeB, CoSm, CoZr and FeMn in 2ICl/13Ar ICP discharges as a function of process pressure.

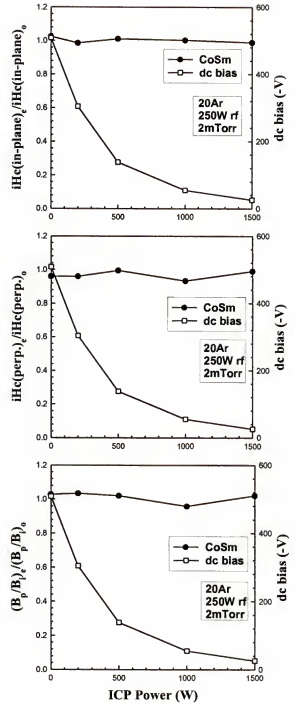

Figure 5-17. Magnetic properties measured with field both in-plane and perpendicular to the film plane of CoSm, as a function of source power, for samples exposed to Ar plasmas at fixed rf chuck power and pressure. The subscript e refers to plasma exposed, the subscript o to the original (unexposed) properties, the subscript i to in-plane fields and the subscript p to perpendicular measurement fields.

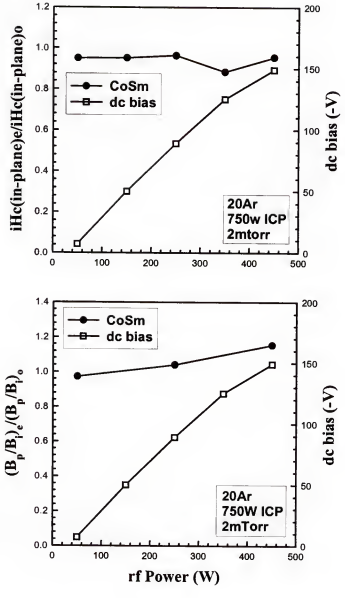

Figure 5-18. Magnetic properties of CoSm, as a function of rf chuck power, for samples exposed to Ar plasma at fixed source power and pressure.

CHAPTER 6
INDUCTIVELY COUPLED PLASMA AND ELECTRON CYCLOTRON RESONANCE PLASMA ETCHING WITH CO/NH_3 CHEMISTRY

6.1. Introduction

The continuing push to higher magnetic recording densities places increasing demand on etching processes capable of producing sub-micron track width poles for write heads.[57-61] In addition there is a need for improved pattern transfer technologies in the fabrication of magnetic random access memories, sensors, actuators and magnetic transducers. Conventional dry etching techniques such as reactive ion etching (RIE) with Cl_2 are generally not applicable to the materials comprising the poles in write heads (which include NiFe or Fe-based materials such as FeAlN and FeTaN)[62] or the sliders in recording heads (Al_2O_3-TiC),[63] due to the low volatility of the etch products. Most of the etching in these applications has been performed with Ar^+ ion milling[60,61] or focused ion beam etching,[12,59] and some selectivity may be achieved by using reactive milling processes based on Ar/O_2 or Ar/N_2.[62] Ion milling suffers from several potential drawbacks, including redeposition onto the feature sidewalls,[64] trenching at the base of the sidewalls and degraded anisotropy of the pattern transfer.[13]

In an attempt to increase the volatility of the magnetic materials etch products, Kinoshita et. al.[18] reported use of elevated substrate temperatures during RIE. While the etch rate at ~380°C was a factor of three larger than pure Ar^+ ion milling, this temperature is unacceptably high for many magnetic structures, particularly multilayers of the type

used in Giant Magnetoresistance (GMR) devices. An alternative method of providing the energy needed to desorb the etch products is use of high ion density plasmas.[35,63] The ion flux in these tools is 2-3 orders of magnitude higher than in RIE systems, and thus it is possible to operate in a regime where there is a balance of etch product formation and the immediate ion-assisted desorption of these products. In this situation there is no build-up of a reaction or selvedge layer on the sample surface, which in RIE actually produces net deposition rather than etching.[46]

While Cl_2-based plasma chemistries operated under high density conditions provide practical etch rates for NiFe and Al_2O_3-TiC, there is always a concern with corrosion caused by plasma residues that remain on feature sidewalls upon removal from the reactor. Nakatani[23] reported use of a non-corrosive CO/NH_3 plasma chemistry for NiFe, in which the etch products are expected to be carbonyls (e.g. $Fe(CO)_5$). The resultant etch rates were $\leq 300 Å \cdot min^{-1}$ for $Ni_{0.8}Fe_{0.2}$, a factor of about three higher than purely physical Ar^+ sputtering under the same conditions. The reactor employed was non-commercial, and might be classified as a magnetron-type, medium ion density system.

In this chapter we report on a parametric investigation of CO/NH_3 etching of NiFe, NiFeCo and related thin film materials using either an Inductively Coupled Plasma (ICP) reactor which is the preferred embodiment of the high density source because of its excellent scalability and uniformity, ease of tuning and absence of bulky, expensive electromagnets or an Electron cyclotron Resonance (ECR) reactor. We find maximum etch rates for NiFe and NiFeCo in the range $350\text{-}400 Å \cdot min^{-1}$ in ICP system and 500 $Å \cdot min^{-1}$ in ECR system, with the rates being a strong function of $CO:NH_3$ ratio, source

and rf chuck power and pressure. We also compared use of CO_2 to replace CO, though this does not appear to offer any advantage in etch rates. Finally, the selectivity for etching the magnetic materials over common mask materials (photoresist, SiO_2) was measured over broad range of conditions.

6.2. Materials and Experimental Procedure

Layers of $Ni_{0.8}Fe_{0.2}$, $Ni_{0.8}Fe_{0.13}Co_{0.07}$, Cu, TaN and CrSi ~5000Å thick were deposited on (100) Si wafers by dc magnetron sputtering. The latter two materials are used as contact or anti-corrosion layers in multilayer magnetic structures, while the Cu is an anti-ferromagnetic coupling material. We also produced very thick (~3μm) $Ni_{0.8}Fe_{0.2}$ layers by electrolytic plating to simulate the structure of write heads. These other materials which are common masks during dry etching, namely photoresist (AZ5209E), bias-sputtered quartz (BSQ) or thermal SiO_2, were included in all experiments so that we could measure the etch selectivity of the metal layers relative to thin prospective masks.

Etching was performed in both Plasma Therm 790 system and Plasma-Therm SLR 770 System. For 790 system, the plasma is generated in a 3-turn, 2MHz, 1500W ICP source. The sample chuck is separately biased with rf power (13.56MHz, 450W) and He backside-cooled. For 770 system, the plasma is generated in an ASTEX 4400 low profile ECR source (2.45GHz).[65] The source power was varied from 400-1000W, with an upper magnet of 170A and a lower collimating magnet current of 40A. Both systems produced the ion density from ~3×10^{10} to $5\times10^{11}cm^{-3}$, as measured by microwave interferometry. The process pressure was varied from 1.5-15mTorr. The gases were

injected directly into the source through electronic mass flow controllers, at a total gas load of ~15 standard cubic centimeters per minute. Etch rates were measured by stylus profilometry after removal of the mask material, while scanning electron microscopy (SEM) was used to examine feature anisotropy. The near-surface chemistry was investigated by Auger Electron Spectroscopy (AES).

6.3. Results and Discussion

6.3.1. Inductively Coupled Plasma Etching

6.3.1.1. Role of plasma chemistry

One of the key results in Nakatani's work was that NH_3 was needed in the plasma chemistry to prevent dissociation of the CO. If the latter occurs,[23] then it would block formation of the metal carbonyl etch products. To examine the species created in ICP sources, optical emission spectroscopy (OES) was employed. Figure 6-1 shows that there is a significant difference in the spectra obtained from CO/NH_3 and CO_2/NH_3 discharges. In the latter case only two dominant lines (486 and 660nm) due to atomic hydrogen are observed. By sharp contrast, the CO/NH_3 spectra is dominated by the NH_3 component, which in turn comprises the N° transitions (300-400nm) and the N_2^+ and N^+ components (550-700nm) together with the atomic H° lines. There is no indication of the dissociation of the CO or CO_2, and for pure discharges of these feed gases we observed only broad molecular continuum.

Figure 6-2 shows etch rates of NiFe and NiFeCo in $2CO/13NH_3$ and $2CO_2/13NH_3$ discharges (250W rf chuck power, 2mTorr process pressure) as a function of source

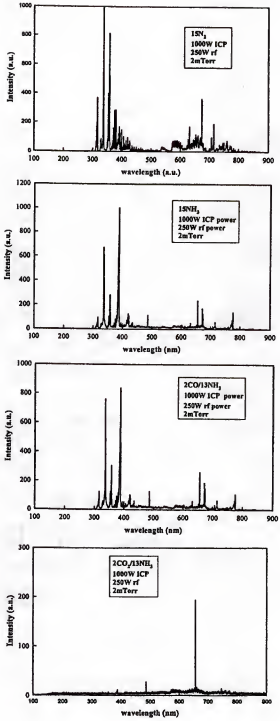

Figure 6-1. Optical emission spectra from N_2, NH_3, CO/NH_3 and CO_2/NH_3 ICP discharges at fixed source power (1000W), rf chuck power (250W) and pressure (2mTorr).

power. Note that at zero watts source power, which corresponds to reactive ion etching, the etch rates are negligible. The rates increase with source power as both the ion flux and plasma dissociation efficiency increases. At the highest powers the rates fall-off, probably due to a combination of reduced ion energy as the plasma conductivity increases and to sputter-desorption of the reactants before they can react with the surface of the magnetic materials. The selectivity for NiFe and NiFeCo over Al_2O_3 under these conditions is ≤40. Note that the CO/NH_3 chemistry produces faster rates than CO_2/NH_3 over a broad range of conditions, presumably because the CO species is the active etchant.

To determine whether there is a significant chemical component to the etching with CO/NH_3, we compared etch rates with purely physical chemistries (Ar and N_2). For these and all subsequent experiments the cathode area was reduced (from 8 to 4 inch diameter) to increase the power density in the plasma and enhance the physical component of the etching. Figure 6-3 shows etch rates of NiFe and NiFeCo in the three plasma chemistries as a function of either source power (top) or rf chuck power (bottom). There is a very clear conclusion from this data-the rates with CO/NH_3 are lower than those with Ar, showing that the chemical enhancement with the former is not large. However a better comparison is between N_2 and CO/NH_3 since the heaviest ion in both mixtures has mass 28 (N_2^+, CO^+). In this comparison, it is seen that there is indeed some chemical enhancement with the CO/NH_3. Note that at high rf powers or source powers we actually observe net deposition on NiFe exposed to N_2 plasmas, possibly due to formation of surface nitrides. Surface analysis by Auger Electron Spectroscopy shows only the presence of the Ni, Fe plus C, O and N.

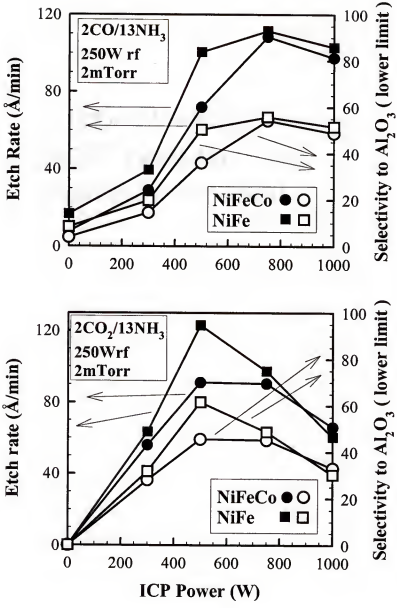

Figure 6-2. Etch rates of NiFe and NiFeCo and selectivity to Al_2O_3 as a function of ICP source power in $2CO/13NH_3$ (top) or $2CO_2/13NH_3$ (bottom) discharges.

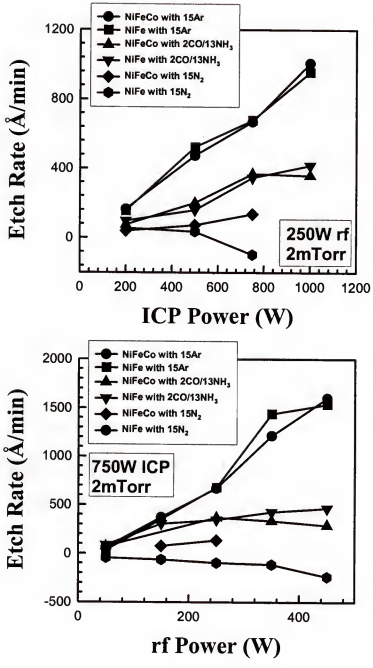

Figure 6-3. Etch rates of NiFe and NiFeCo as a function of source power (top) or rf chuck power (bottom) in ICP N_2, Ar, CO/NH_3 discharges.

6.3.1.2. Effect of plasma parameters

Each of the main plasma parameters was systematically varied to determine the effect on $Ni_{0.8}Fe_{0.2}$ etch rate and the selectivity relative to SiO_2, which as we will see later is the most appropriate mask material. Figure 6-4 shows the effect of CO percentage in the discharge (top) and of process pressure (bottom). The NiFe etch rate initially increases as CO is added to the discharge, but then decreases at CO-rich conditions. This is consistent with the result from Nakatani[23] that NH_3 is needed to assist in the formation of the metal carbonyls. The etch selectivity relative to SiO_2 depends on the how the SiO_2 was produced-thermal oxide has significantly lower etch rate than deposited oxide and consequently produces higher selectivity for NiFe over SiO_2. Similar trends are observed with process pressure-initially the NiFe etch rate increases as more reactants are available, but above ~2mTorr the rates decrease due to increased recombination in the discharge.

Figure 6-5 shows the effect of source power (top) and rf chuck power (bottom) at fixed discharge composition. The same trend as discussed earlier for lower CO contents (Figure 6-2, where $2CO/13NH_3$ discharges were employed) were observed, with the etch rates decreasing at high source powers. The fact that the etch mechanism is still physically dominated is clear from the lower part of the Figure, where the NiFe etch rate increases monotonically with rf power. Note that selectivities in the range 5-8 are obtained relative to thermal SiO_2.

The effect of substrate temperature is shown in Figure 6-6. The NiFe etch rate continues to increase with temperature as the vapor pressure of the metal carbonyls increases and they are more effectively removed from the surface. A rate of $400Å \cdot min^{-1}$

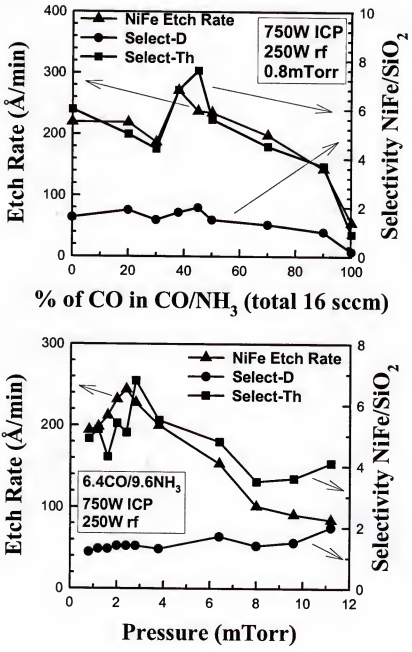

Figure 6-4. Etch rates of NiFe and deposited (D) or thermal (Th) SiO_2 as a function of either CO percentage (top) or process pressure (bottom) in ICP CO/NH_3 discharges.

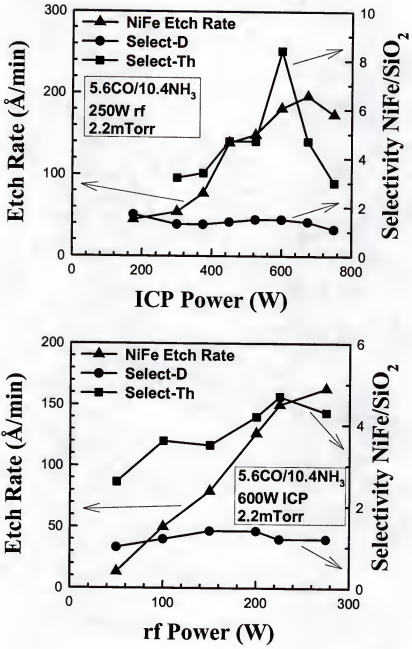

Figure 6-5. Etch rates of NiFe and deposited (D) or thermal (Th) SiO_2 as a function of either ICP source power (top) or rf chuck power (bottom) in ICP CO/NH_3 discharges.

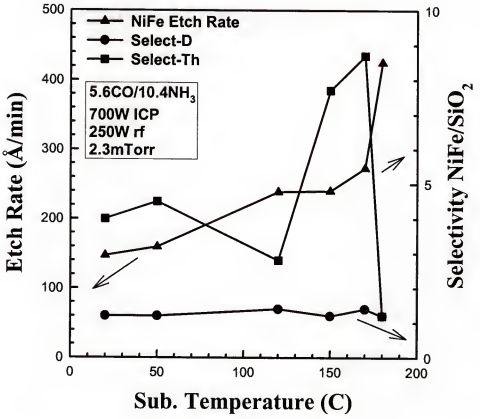

Figure 6-6. Etch rates of NiFe and deposited (D) or thermal (Th) SiO_2 as a function of substrate temperature in ICP CO/NH_3 discharges.

was obtained at 175°C, where the selectivity to thermal oxide falls off rapidly to the value for deposited oxide. Note that selectivities are ≤10 in all cases for both oxides.

6.3.1.3. Etching of typical magnetic multilayer materials

The new generations of magnetic memories and storage devices are based on GMR multilayers comprising materials such as NiFe, NiFeCo, TaN, Cu and CrSi[57,60]. A key question is whether the CO/NH_3 plasma chemistry can also etch the latter three materials. Figure 6-7 shows the effect of source power (top) and rf chuck power (bottom) on material etch rates. While Cu etches faster than NiFe, the rates for both TaN and CrSi are basically just due to physical sputtering and there is no chemical component to their removal mechanism. For the type of GMR structures used for magnetic recording, the individual layers are only 50-250Å thick, and therefore etch rates of $100Å \cdot min^{-1}$ are probably acceptable.

As mentioned earlier photoresist does not hold up well in the CO/NH_3 discharges. Some typical etch rate data is shown in the top part of Figure 6-8 for variation of source power. The photoresist typically etches at a rate 10-20 times faster than NiFe and NiFeCo. By contrast, the etch rates for SiO_2 are much lower (some typical data are shown in the lower part Figure 6-8 for variation of rf chuck power), indicating that this is the most appropriate mask material.

For a typical GMR multilayer (CrSi/NiFe/Cu/NiFeCo/TaN) with total thickness ~2,000Å, the CO/NH_3 chemistry can provide clean, effective pattern transfer using SiO_2 masks, as shown in the SEM micrograph of Figure 6-9. Even though the etching is still physically-dominated, the etch time is short enough that mask erosion is not significant.

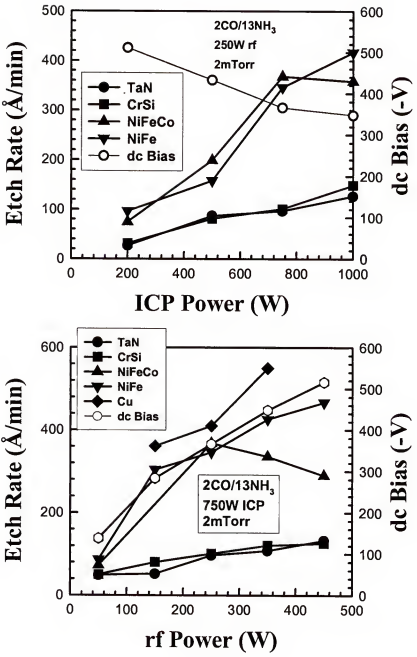

Figure 6-7. Etch rates of NiFe, NiFeCo, TaN, CrSi and Cu as a function of either ICP source power (top) or rf chuck power (bottom) in ICP CO/NH_3 discharges.

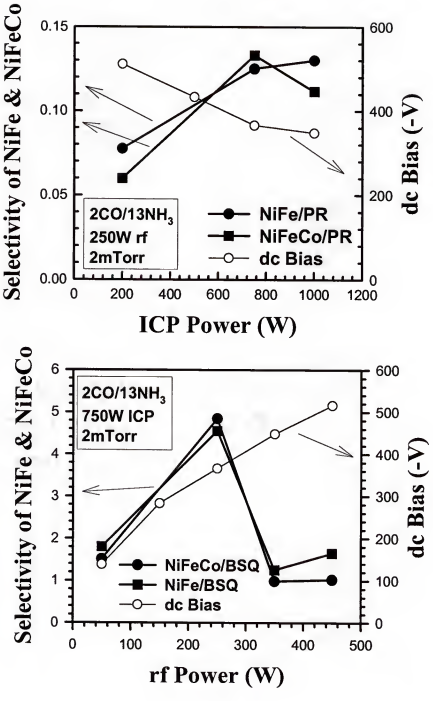

Figure 6-8. Etch selectivity for NiFe and NiFeCo over photoresist (top) or bias sputter deposited quartz (BSQ) as a function of either ICP source power (top) or rf chuck power (bottom) in ICP CO/NH_3 discharges.

Figure 6-9. SEM micrograph of features etched into a CrSi/NiFe/Cu/NiFeCo/TaN multilayer structure using an ICP CO/NH_3 discharge. The 3000Å thick SiO_2 mask is still in place.

There was no long-term (3 months) corrosion observed on these samples, as expected due to the non-corrosive nature of the plasma chemistry.

By contrast, if very deep (>1μm) etch depths are required, then erosion of the SiO_2 mask becomes noticeable. Figure 6-10 shows features etched ~1μm deep into NiFe using CO/NH_3. The dimpling on the mask area was not a result of the plasma etch process, but was visible on the pre-etched samples. Facetting of the SiO_2 mask leads to sloped, rough sidewalls on the etched features, and will present a sever problem for making small-dimension structures.

6.3.2. Electron Cyclotron Resonance Plasma Etching

6.3.2.1. Role of plasma chemistry

Figure 6-11 compares NiFe and NiFeCo etch rates in CO/NH_3 (top) and CO_2/NH_3 (bottom) ECR discharges (750W source power, 250W rf chuck power, 2mTorr pressure) as a function of discharge composition. There are significant differences in behavior between the two chemistries, but they display the same basic trend of increase in etch rate as CO or CO_2 is initially added to the discharge, followed by a fall-off to net deposition at low NH_3 compositions. The initial etch rate increase as CO or CO_2 is added is indicative of some degree of chemical enhancement due to these gases, which was confirmed by a comparison with pure N_2 discharges. The heaviest ion in N_2 or CO/NH_3 discharges should have mass 28 (N_2^+ or CO^+). (It is possible in some cases to have ion-molecule reactions with large cross-sections can give molecular ions such as I_3^+ in iodine-containing discharges. However the gas mixtures in this study are unlikely to give any molecular

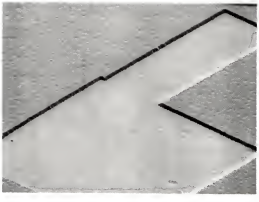

15KV ×1000 10.0μm UFMSE

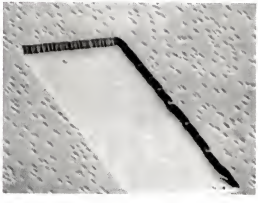

15KV ×2200 10.0μm UFMSE

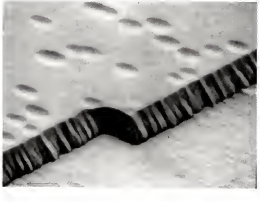

15KV ×7800 1.0μm UFMSE

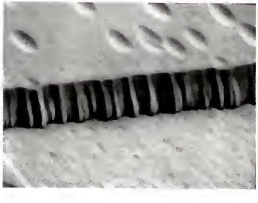

15KV ×10000 1.0μm UFMSE

Figure 6-10. SEM micrographs of features etched into a thick NiFe layer using an ICP CO/NH_3 discharge. The 5000Å thick SiO_2 mask is still in place, and little was lost on the field during the etch process.

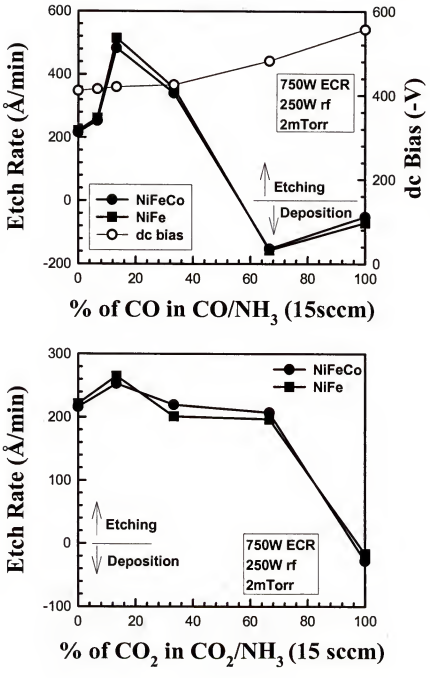

Figure 6-11. Etch rates of NiFe and NiFeCo in CO/NH_3 (top) or CO_2/NH_3 (bottom) discharges (750W source power, 250W rf chuck power) as a function of plasma composition.

ions heavier than additional hydrogen attachment to CO^+). A sputter rate for NiFe of ~350Å·min^{-1} was obtained for pure N_2 discharges under these conditions, which is less than the maximum rate obtained using CO/NH_3. By analogy with the work of Nakatani,[23] the fact that the process reverts to net deposition at high CO or CO_2 concentrations may be due to the creation of a carbided surface. Some evidence for this comes from the AES surface scans of Figure 6-12. After exposure to a CO/NH_3 plasma at conditions where there is net deposition, there is additional C and N detected on the surface due to polymer or carbide formation that prevents etching.

We could not detect any measurable differences in the optical emission spectra from pure CO and CO_2 discharges (Figure 6-13). There appears to be a line at ~780nm due to atomic oxygen. Unfortunately many of the CO and CO_2 transitions are below 300nm, where our spectra are cut-off by the quartz viewport on our system. As NH_3 is added to the discharge (Figure 6-13, bottom), there is the appearance of atomic hydrogen transitions at 480 and 660nm and the nitrogen-related bands between 300-400nm. At NH_3-rich conditions where etching of the magnetic materials occur, the spectra is completely dominated by N_2 and H transitions. Therefore optical emission spectroscopy does not appear that useful for tracking the active species in the plasma.

6.3.2.2. Effect of plasma parameters

Figure 6-14 shows the effect of microwave source power on the etch rates of NiFe and NiFeCo for two different plasma compositions at fixed rf chuck power (250W) and process pressure (2mTorr). At low CO to NH_3 ratios (2/13) the etch rates increase with source power (which controls ion flux and dissociation of the discharge) and then

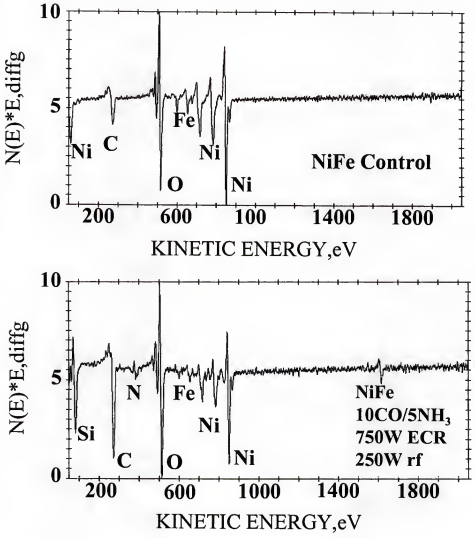

Figure 6-12. AES surface scans of NiFe before (top) and after (bottom) etching in $10CO/5NH_3$ discharges (750W source power, 250W rf chuck power). The Si signal in the latter case comes from the edge of the sample where the substrate is exposed.

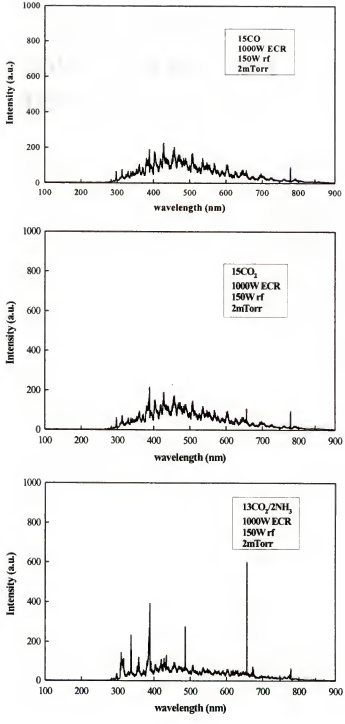

Figure 6-13. Optical emission spectra of CO (top), CO_2 (center) or CO/NH_3 ECR discharges (1000W source power, 250W rf chuck power, 2mTorr).

decrease beyond ~750W. The dc self-bias decreases as plasma conductivity increases, but the fall-off in etch rate at high source power is most likely due to the onset of surface carbidation. This would be consistent with the data in the lower part of the Figure, where a transition to net deposition occurs at much lower source powers in CO-rich discharges.

The role of ion energy on the NiFe and NiFeCo etch rates is shown in Figure 6-15. The sum of dc self-bias and plasma potential (~-25eV in this tool) is the average energy for ions striking the sample.[34] As rf chuck power is increased the dc self-bias increases, but the etch rates fall-off above particular ion energies (~450eV for the $2CO/13NH_3$ condition and ~400eV for the $10CO/5NH_3$ condition). This is often observed in high density plasma etching,[36] and is usually ascribed to desorption of the reactive neutrals by ion-assistance before they can react with the sample surface. In the CO/NH_3 chemistry the high ion energy conditions may also lead to dissociation of the adsorbed CO species, because the process reverts to net deposition under CO-rich conditions.

Examples of the effect of process pressure are shown in Figure 6-16 for two different plasma compositions at fixed source power (750W) and rf chuck power (250W). For NH_3-rich conditions (top) the etch rates for Ni and NiFeCo decrease with increasing pressure as recombination in the plasma becomes more important. For CO-rich conditions (bottom) there is a transition from deposition to etching, followed by the same decrease in etch rates at higher pressure. These results emphasize the importance of balancing ion flux and reactive neutral concentration in order to optimize the NiFe and NiFeCo etch rates in the CO/NH_3 plasma chemistry and may be an additional reason why most attempts in the past at using CO-based mixtures have been unsuccessful.

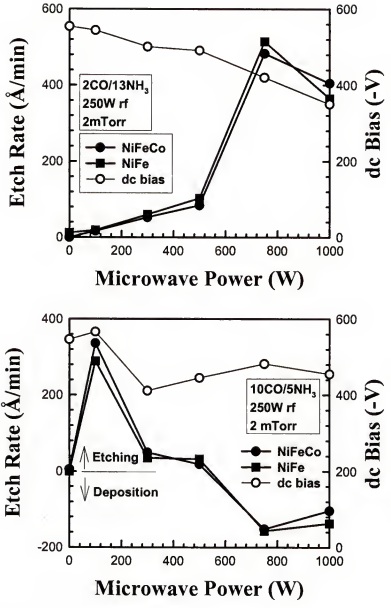

Figure 6-14. Etch rates of NiFe and NiFeCo in $2CO/13NH_3$ (top) or $10CO/5NH_3$ (bottom) discharges (250W rf chuck power, 2mTorr) as a function of microwave source power.

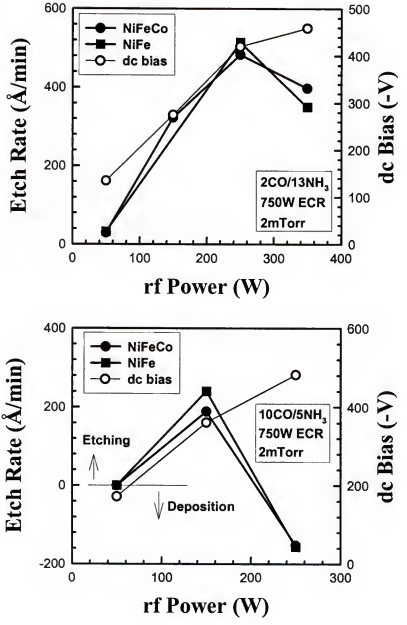

Figure 6-15. Etch rates of NiFe and NiFeCo in $2CO/13NH_3$ (top) or $10CO/5NH_3$ (bottom) discharges (750W source power, 2mTorr) as a function of rf chuck power.

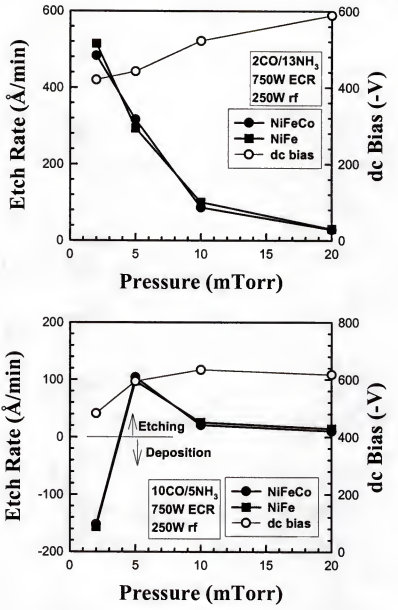

Figure 6-16. Etch rates of NiFe and NiFeCo in $2CO/13NH_3$ (top) or $10CO/5NH_3$ (bottom) discharges (750W source power, 250W rf chuck power) as a function of process pressure.

Since there is a still a need to have a strong physical component to the etching, mask erosion (i.e. facetting leading to sloped sidewalls) is a problem when long etch times are needed. However for relatively shallow etch depths, mask erosion is less of an issue and quite impressive pattern transfer into NiFe (or NiFeCo) can be achieved with the CO/NH_3 mixture. Figure 6-17 shows SEM micrographs of features etched into NiFe using a $2CO/13NH_3$, 750W source power, 250W rf chuck power, 2mTorr discharge. The sidewalls are smooth and vertical, but there is some rounding of the mask edges due to erosion during the plasma exposure.

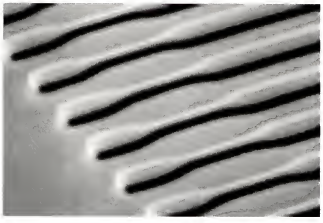

Figure 6-17. SEM micrographs of features etched into NiFe layers using a $2CO/13NH_3$ discharge (750W source power, 250W rf chuck power, 2mTorr). The SiO_2 mask is still in place.

CHAPTER 7
SUMMARY

The etching characteristics of magnetic materials such as NiFe, NiFeCo, and other related materials were investigated in various plasma chemistries and different high density plasma reactors, namely Inductively Coupled Plasma (ICP) reactor and Electron Cyclotron Resonance (ECR) Plasma reactor. The characteristics for each plasma chemistry are summarized in Table 7-1. The main point of this research is that both tools are more efficient in patterning those materials, in comparison with conventional plasma etching techniques such as Reactive Ion Etching (RIE) or Ion Milling.

High rate etching of NiFe and NiFeCo is possible at ≤80°C under high density ECR plasma conditions by balancing the ion-neutral ratio and preventing the formation of a selvedge layer. The high ion flux essentially provides the impetus for etching, replacing the need for the elevated sample temperatures (≤200°C) necessary under conventional RIE conditions. The ECR tool has much higher rates for our conditions, but there is evidence this is a result of its smaller electrode area and consequent higher power density. A consequence of the requirement for high ion fluxes is that photoresist is not a suitable mask material, and dielectrics such as SiO_2 and SiN_X must be employed. Post-etch corrosion of the NiFe and NiFeCo may be avoided by using an in-situ H_2 plasma clean, but this is dependent on the prior history of the reactor chamber.

ICP etching in Cl_2/Ar discharges is effective for pattern transfer in NiFe, NiFeCo, CrSi and TaN, the basic components of MRAM stacks. The etch rates are a strong

function of the ion-to-neutral ratio incident on the surface, and this is affected by process pressure, discharge composition, ion energy and ion flux (i.e. rf chuck power and ICP source power). The use of Ar addition is more effective than either N_2 or H_2 in obtaining the fastest etch rates, and dielectric masks are more stable than photoresists.

Etching of NiFe and NiFeCo has been performed in ICP Cl_2/He, Cl_2/Ar and Cl_2/Xe discharges to compare with the effectiveness of He, Ar and Xe additives to ICP Cl_2 plasmas for etching NiFe and NiFeCo. The etch rates go through a maximum with rf chuck power and source power, reflecting the need to balance ion flux, neutral density and ion energy in order to optimize the formation and desorption of the chloride etch products. The smoothest surfaces in both NiFe and NiFeCo were obtained with the Cl_2/He chemistry under our conditions, corresponding to the lowest amount of residual chlorine.

The effect of the inert gas additive to Cl_2 plasmas during etching of CoFeB, CoZr, CoSm and FeMn was also investigated. The absolute rates scale with atomic weight of the additive species, and the smoothest surfaces were obtained with Ar and Xe addition. The etch rates go through maxima with discharge composition and rf chuck power, and a transition from net desorption to etching with source power and rf chuck power. These trends reflect the need to balance ion flux, chlorine atomic neutral density and ion energy in etching magnetic materials. The key is to find the parameter space in which the formation and desorption of the metal chloride etch products is balanced.

ICP etching does not have any measurable effect on the magnetic quality of thin film Ni, NiFe or NiFeCo, with any "dead layers" being <50Å in thickness. Similarly, ICP-etched MRAM multilayer stacks show no change in magnetic properties from thin

control values, provided chlorine residues are removed. Post-etch rinsing in H_2O or in-situ plasma cleaning with H_2, O_2 or SF_6 discharges are all effective treatments for removing chlorine etch residues. Of these, only O_2 plasma exposure appears to degrade the magnetic properties of MRAM stacks. Once the residues are removed, there is no change in magnetic or visual properties over a period of ~6months (extent of our study). The combination of Cl_2/Ar ICP etching and post-etch cleaning provides an effective pattern transfer method for magnetic multilayers.

The interhalogen compounds ICl and IBr are effective dry etchants for Ni, Fe, NiFe and NiFeCo under high ion density conditions. The maximum etch rates are similar to those we have achieved with pure Cl_2 under the same conditions in the same reactor, but the surfaces are smoother over a broader range of conditions than with Cl_2 (which typically produced RMS values a factor of 2-3 higher). This appears to be related to the lower amount of residual halogen on the etched surfaces (our past results with Cl_2 typically show 1-3 at.% chlorine residues). The etch rates are strongly dependent on plasma composition, source power, rf chuck power and pressure. All of these trends with plasma parameters are consistent with the etching being limited by the removal of the halogenated reaction products, and the need to balance the formation and removal of these species.

ICl and IBr discharges operated under Inductively Coupled Plasma conditions also provide effective etching of CoFeB, CoSm, CoZr and FeMn. Higher etch rates were obtained for CoSm, CoZr and FeMn with both interhalogens relative to Cl_2 discharges under the same conditions. There was no degradation of magnetic properties of etched CoSm films.

Table 7-1. Typical results for the etching of NiFe in High-Density Plasma Reactor.

CHEMISTRY	TYPICAL ETCH RATES	CORROSIVE	COMMENTS
Cl_2/Ar	600Å·min^{-1} ICP >1000Å·min^{-1} ECR	YES	• CHEMICAL ENHANCEMENT OF 100% • ETCH RATE WITH Xe>Ar>He
CO/NH_3	250Å·min^{-1} ICP 500Å·min^{-1} ECR	NO	• CHEMICAL ENHANCEMENT OF ~20%-40% • CO_2 LESS EFFECTIVE THAN CO
CH_4/H_2/Ar	<100Å·min^{-1}	NO	• SLOWER THAN Ar SPUTTERING
SF_6/Ar	<100Å·min^{-1}	NO	• SLOWER THAN Ar SPUTTERING
BI_3/Ar	500Å·min^{-1}	YES	• LESS EFFECTIVE THAN Cl_2/Ar
BBr_3/Ar	200Å·min^{-1}	YES	• SLOWER THAN Ar SPUTTERING
ICl/Ar	500Å·min^{-1}	YES	• EXECLLENT SURFACE MORPHOLOGY
IBr/Ar	500Å·min^{-1}	YES	• EXECLLENT SURFACE MORPHOLOGY

A systematic study of ICP and ECR etching of NiFe, NiFeCo and related magnetic materials in the CO/NH_3 plasma chemistry has revealed. The following:

1. There is a small chemical component present with this chemistry, as determined by a comparison with N_2 sputtering.
2. The plasma needs to be NH_3-rich in order to produce the highest etch rates.
3. There is no advantage to replacing CO with CO_2.
4. The chemistry needs to be operated under high density conditions to achieve practical etch rates.
5. Photoresist is not an acceptable mask material, but SiO_2 holds up well for shallow etch depth ($\leq 0.5\mu m$) applications.
6. The etch rates are a strong function of ion flux, ion energy, pressure and substrate temperature.

REFERENCES

1. G. A. Prinz, in Ultra-Thin Magnetic Structures II, ed. B. Heinrich and J. A. C. Bland (Springer-Verlag, Berlin, 1994)

2. C. H. Tsang, R. E. Fontana, Jr., T. Lin, D. E. Heim, B. A. Gurney and M. L. Williams, IBM J. Res. Develop. 42 103 (1998).

3. C. H. Tsang, J. Appl. Phys. 69 5393 (1991).

4. R. White, IEEE Trans. Magn. 28 2482 (1992).

5. J. M. Daughton, P. Bade, M. Jenson and M. Rahmati, IEEE Trans Magn. 28 2488 (1992).

6. D. E. Heim, R. E. Fontana, Jr., C. H. Tsang, V. Speriosu, B. A. Gurney and M. L. Williams, IEEE Trans. Magn. 30 316 (1994).

7. M. Parker, K. Coffrey, J. Howard, C. H. Tsang, R. E. Fontana, Jr. and T. Hylton, IEEE Trans. Magn. 32 142 (1996).

8. R. E. Fontana, S. MacDonald, C. H. Tsang and T. Lin, IEEE Trans. Magn. 32 3440 (1996).

9. B. A. Everitt, A. V. Pohm and J. M. Daughton, J. Appl. Phys. 81 23639 (1997).

10. S. Wang, F. Liu, K. D. Maranowski and M. H. Kryder, IEEE Trans. Magn. 26 1689 (1989).

11. S. Wang, E. Louis, F. Wolfson, R. Anderson and M. H. Kryder, IEEE Trans. Magn. 30 3897 (1994).

12. H. Takano, H. Fukuoka, M. Suzuki, K. Shiiki and M. Kitadu, IEEE Trans. Magn. 27 4678 (1991).

13. H. Gokan and S. Eho, J. Vac. Sci. Technol. 18 23 (1991).

14. M. J. Vasile and C. J. Mogab, J. Vac. Sci. Technol. A 4 1841 (1986).

15. R. Giridhar, Jpn. J. Appl. Phys. 35 6347 (1996).

16. C. Tsang, M. Chen, T. Yogi and K. Ju, IEEE Trans. Magn. 30 281 (1994).

17. F. C. M. J. van Delft, J. Magn. Mag. Mat. 140-144 2203 (1995).

18. K. Kinoshita, K. Yamada and H. Matutera, IEEE Trans. Magn. 27 4888 (1991).

19. M. Balooch, D. S. Fischl, D. R. Olander and W. J. Siekhaus, J. Electrochem. Soc. 135 2090 (1988).

20. D. S. Fischl and D. W. Hess, J. Vac. Sci. Technol. B 6 1577 (1988).

21. D. W. Hess, Plasma Chem. Plasma Proc. 2 141 (1982).

22. B. Khamsehpour, C. D. W. Wilkinson and J. N. Chapman, Appl. Phys. Lett. 67 3194 (1995).

23. I. Nakatani, IEEE Trans. Magn. 32 4448 (1996).

24. P. M. Levy, J. of Magnet. and Magnet Mater, Vol. 140-44, 485 (1995).

25. P. M. Levy, Solid State Physics, Vol. 47, 367-462 (1994).

26. See for example, IBM Storage Division Web-Site, http://www.storage.ibm.com/hardsoft/diskdrdl/technolo/gmr/gmr.htm

27. B. El-Kareh, Fundamentals of Semiconductor Processing Technology. Kluwer Academic Publishers, Boston, 1995.

28. D. M. Manos and D. L. Flamm, Plasma Etching: An Introduction. Academic Press, Boston, 1989.

29. P. Singer, Semiconductor International, 154 (July 1996).

30. B. Gorowitz, R. J. Saia and E. W. Balch, in VLSI Electronics Microstructural Science, ed. N. G. Einspruch, S. S. Cohen and G. Gildenblat, Vol 15 (Academic Press, Orlando 1987) Chapter 4.

31. A. K. Sinha, H. S. Lindenburger, D. B. Fraser, S. P. Murarka and E. N. Fuls, IEEE Trans. Electron Dev. ED-27 1425 (1980).

32. T. M. Mayer, J. M. E. Harper and J. J. Cuomo, J. Vac. Sci. Technol. A 3 1779 (1985).

33. CRC Handbook of Chemistry and Physics 72nd Edition (CRC Press, Boca Raton, FL 1989).

34. M. A. Liebermann and A. J. Lichtenburg, Principles of Plasma Discharges and Materials Processing (John Wiley and Sons, NY 1994).

35. K. B. Jung, E. S. Lamber, J. R. Childress, S. J. Pearton, M. Jenson and A. T. Hurst, Jr., Appl. Phys. Lett. 71 1255 (1997).

36. S. J. Pearton, T. Nakano and R. A. Gottscho, J. Appl. Phys. 69 4206 (1991).

37. R. J. Shul, M. L. Lovejoy, D. L. Hetherington, D. J. Rieger, J. F. Klem and M. R. Melloch, J. Vac. Sci. Technol. B 13 27 (1995).

38. R. J. Davis and E. D. Wolf, J. Vac. Sci. Technol. B 8, 1798 (1990).

39. G. S. Oehrlein, Y. Zheng, D. Vender and O. Joubert, J. Vac. Sci. Technol. A 12, 323 (1994).

40. J. Mau, J. Vac. Sci. Technol. B 6, 652 (1987).

41. D. A. Danner, M. Dalvie and D. W. Hess, J. Electochem. Soc. 134, 669 (1987).

42. J. W. Lee, J. Hong and S. J. Pearton, Appl. Phys. Lett. 68 847 (1996).

43. S. J. Pearton, J. W. Lee, E. S. Lambers, J. R. Mileham, C. R. Abernathy, F. Ren, W. S. Hobson and R. J. Shul, J. Vac. Sci. Technol. B 14 118 (1996).

44. F. Ren, W. S. Hobson, J. R. Lothian, J. Lopata, J. A. Caballero, S. J. Pearton and M. W. Cole, Appl. Phys. Lett. 67 2497 (1995).

45. J. W. Lee, J. Hong, E. S. Lambers and S. J. Pearton, J. Vac. Sci. Technol. B 15 652 (1997).

46. K. B. Jung, E. S. Lambers, J. R. Childress, S. J. Pearton, M. Jenson and A. T. Hurst, Jr., J. Vac. Sci. Technol. A 16 1697 (1998).

47. K. B. Jung, J. Hong, H. Cho, J. R. Childress, S. J. Pearton, M. Jenson and A. T. Hurst Jr., J. Electron. Mat. 27 972 (1998).

48. See example, High Density Plasma Sources, ed. O. A. Popov (Noyes Publications, Park Ridge, NJ 1994).

49. Y. B. Hahn (to be published).

50. B. Vavra, Honeywell SSEC, Plymouth, MN (private communication).

51. See for example, G. S. Oehrlein and Y. Kurogi, Mat. Sec. Eng. R 24 153 (1998).

52. J. M. Daughton, Thin Solid Films 216 162 (1992).

53. T. Osaka, T. Homma, K. Saito, A. Takekoshi, Y. Yamazuki and T. Namikawa, J. Electrochm. Soc. 139 1311 (1992).

54. M. Jimbo, K. Komiyama and S. Tsunashima, J. Appl. Phys. 79 6237 (1996); J. Magn. Mag. Mater. 165 308 (1997).

55. J. A. Caballero, W. J. Geerts, F. Petroff, J. –V. Thiele, D. Weller and J. R. Childress, J. Magn. Mag. Mater. 177-181 1229 (1998).

56. K. B. Jung, H. Cho, Y. B. Hahn, D. C. Hays, T. Feng, Y. D. Park, J. R. Childress and S. J. Pearton, Mat. Sci. Eng. B. (to be published).

57. H. Yoda, H. Iwasaki, T. Kobayashi, A Tsutai and M. Sahashi, IEEE Trans. Magn. 32 3363 (1996).

58. H. Kanai, K. Yamada, K. Aoshima, Y. Ohtsuku, J. Kane, M. Kanamine, J. Toda and Y. Mizoshita, IEEE Trans. Magn. 32 3368 (1996).

59. W. P. Jayasekara, S. Wang and M. H. Kryder, J. Appl. Phys. 79 5880 (1996).

60. C. H. Tsang, T. Lin, S. MacDonald, N. Robertson, S. Santini, M. Duerner, T. Reith, L. Vo, T. Diola and P. Arnett, IEEE Tras. Magn. 33 2866 (1997).

61. K. Fukuda, M. Sakai, N. Yamanaka, A. Iijima and M. Matsuzaki, IEEE Trans. Magn. 30 3891 (1994).

62. W. P. Jayasekara, J. Grant, J. A. Bain, A. E. T. Kuiper and M. H. Kryder, IEEE Trans. Magn. 33 2830 (1997).

63. N. Fukushima, H. Katai, T. Wada and Y. Horiike, Jap. J. Appl. Phys. 35 2512 (1996).

64. R. E. Lee, J. Vac. Sci. Technol. 16 164 (1979).

65. J. W. Lee, S.J. Pearton, C. J. Santana, J. R. Mileham, E. S. Lambers, C. R. Abernathy, F. Ren and W. S. Hobson, J. Electrochem. Soc. 143 1093 (1996).

BIOGRAPHICAL SKETCH

Kee Bum Jung was born on May 14, 1967, in Seoul, Korea. After graduation from high school, Kee Bum enrolled in the College of Engineering at Inha University in Incheon, Korea, majoring in applied physics. Throughout his years at the university, Kee Bum received an academic scholarship for his outstanding achievements. After Kee Bum received his bachelor's degree in February 1990, he joined the Korea Air Force and served for more than three years as a First Lieutenant and system officer at the Master Control and Reporting Center.

Kee Bum enrolled at the University of Florida in the Department of Electrical Engineering in 1994 and received his master's degree in May 1996. He decided to continue his education for a Ph. D. degree in materials science and engineering. He was very fortunate to meet Professor Pearton and to do research in the development of the dry etching process for magnetic devices. Under Professor Pearton's close supervision and expert guidance, Kee Bum was the author of 36 published technical papers and five conference papers, and has been a member of The Minerals, Metals and Materials Society, American Vacuum Society, Materials Research Society, and American Physical Society.

Kee Bum has accepted a postdoctoral position at IBM Almaden Research Center in San Jose, CA, and wishes to continue to be actively involved in productive research,

building on the foundation of five years of valuable experience at the University of Florida.

I certify that I have read this study and that in my opinion it conforms to acceptable standards of scholarly presentation and is fully adequate, in scope and quality, as a dissertation for the degree of Doctor of Philosophy.

Stephen J. Pearton, Chairman
Professor of Materials Science and Engineering

I certify that I have read this study and that in my opinion it conforms to acceptable standards of scholarly presentation and is fully adequate, in scope and quality, as a dissertation for the degree of Doctor of Philosophy.

Cammy R. Abernathy
Professor of Materials Science and Engineering

I certify that I have read this study and that in my opinion it conforms to acceptable standards of scholarly presentation and is fully adequate, in scope and quality, as a dissertation for the degree of Doctor of Philosophy.

Rajiv K. Singh
Professor of Materials Science and Engineering

I certify that I have read this study and that in my opinion it conforms to acceptable standards of scholarly presentation and is fully adequate, in scope and quality, as a dissertation for the degree of Doctor of Philosophy.

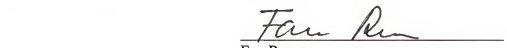

Fan Ren
Associate Professor of Chemical Engineering

I certify that I have read this study and that in my opinion it conforms to acceptable standards of scholarly presentation and is fully adequate, in scope and quality, as a dissertation for the degree of Doctor of Philosophy.

Fred Sharifi
Associate Professor of Physics

This dissertation was submitted to the Graduate Faculty of the College of Engineering and to the Graduate School and was accepted as partial fulfillment of the requirements for the degree of Doctor of Philosophy.

August 1999

M. J. Ohanian
Dean, College of Engineering

Winfred M. Phillips
Dean, Graduate School